LNOx Emission Model for Air Quality & Climate Studies Using Satellite Lightning Mapper Observations

Yuling Wu[1], Arastoo Pour Biazar[2], William J. Koshak[3], and Peiyang Cheng[2]

[1]University of Alabama - Huntsville
[2]University of Alabama in Huntsville
[3]NASA/MSFC

November 22, 2022

Abstract

A lightning nitrogen oxides (LNOx) emissions model using satellite-observed lightning optical energy is introduced for utilization in Air Quality modeling systems. The effort supports assessments of air-quality/climate coupling as related to the influence of LNOx on atmospheric chemistry. The Geostationary Lightning Mapper (GLM), International Space Station Lightning Imaging Sensor (ISS-LIS), and the Tropical Rainfall Measuring Mission (TRMM) LIS data are used to examine the efficacy of the method, extend the previously derived LNOx record, and demonstrate a path for using ISS-LIS observations to cross-calibrate regional LNOx estimates from the future global constellation of geostationary lightning observations. A detailed evaluation of the GLM dataset is provided to establish the robustness of observations for LNOx estimates and to make preliminary assessments of the LNOx emissions model. Seasonal and geographical variation, land/ocean contrast, and annual fluctuation in the GLM observed lightning activity and flash optical energy are provided. GLM detection substantially degrades with the increase in the field of view, resulting in 44% more flashes and 40% less optical energy observation by GLM-16 (compared to GLM-17) to the east of the middle-longitude between the two mappers (106.2°W). Regular horizontal striations are found in the optical energy product. On average, GLM flashes matched to the cloud-to-ground flashes have ˜30% longer duration, 50-70% more extension, and [?] 100% higher optical energy compared to the unmatched flashes (assumed to be intra-cloud). The results from summer-long chemical transport simulations using LNOx generated from the emission model agrees with previous studies and shows consistency across the GLM/LIS datasets.

Hosted file

`essoar.10511778.1.docx` available at https://authorea.com/users/538741/articles/599690-lnox-emission-model-for-air-quality-climate-studies-using-satellite-lightning-mapper-observations

Y. Wu[1], A. Pour-Biazar[1], W. J. Koshak[2], P. Cheng[3]

[1]Earth System Science Center, University of Alabama in Huntsville, Huntsville, AL, USA

[2]Earth Science Branch, NANA Marshall Space Flight Center, Huntsville, AL, USA

[3]Department of Atmospheric and Earth Science, University of Alabama in Huntsville, Huntsville, AL, USA

Corresponding author: Yuling Wu (wuy@nsstc.uah.edu)

Key Points:

- GLM data evaluation
- Geographical and temporal variation of lightning activity
- Satellite lightning observation-based LNOx emission model for air quality and climate studies

Abstract

A lightning nitrogen oxides (LNOx) emissions model using satellite-observed lightning optical energy is introduced for utilization in Air Quality modeling systems. The effort supports assessments of air-quality/climate coupling as related to the influence of LNOx on atmospheric chemistry. The Geostationary Lightning Mapper (GLM), International Space Station Lightning Imaging Sensor (ISS-LIS), and the Tropical Rainfall Measuring Mission (TRMM) LIS data are used to examine the efficacy of the method, extend the previously derived LNOx record, and demonstrate a path for using ISS-LIS observations to cross-calibrate regional LNOx estimates from the future global constellation of geostationary lightning observations. A detailed evaluation of the GLM dataset is provided to establish the robustness of observations for LNOx estimates and to make preliminary assessments of the LNOx emissions model. Seasonal and geographical variation, land/ocean contrast, and annual fluctuation in the GLM observed lightning activity and flash optical energy are provided. GLM detection substantially degrades with the increase in the field of view, resulting in 44% more flashes and 40% less optical energy observation by GLM-16 (compared to GLM-17) to the east of the middle-longitude between the two mappers (106.2°W). Regular horizontal striations are found in the optical energy product. On average, GLM flashes matched to the cloud-to-ground flashes have ~30% longer duration, 50-70% more extension, and 100% higher optical energy compared to the unmatched flashes (assumed to be intra-cloud). The results from summer-long chemical transport simulations using LNOx generated from

the emission model agrees with previous studies and shows consistency across the GLM/LIS datasets.

Introduction

Lightning-induced NOx generation accounts for about 70% of NO_x ($NO + NO_2$) in the upper troposphere (UT) (Schumann and Huntrieser, 2007; Nault et al., 2017; Zhu et al., 2019; Lapierre et al., 2020). NOx is a key precursor of ozone, and its reactions associated with ozone (and OH radical) dominate the tropospheric photochemistry. Lightning NOx (LNOx) plays an important role in regulating UT oxidation capacity and production of ozone, which not only is a critical air pollutant but also a greenhouse gas with substantial radiative effects (Myhre et al., 2014; Sicard, 2021).

The main uncertainty in reflecting the impact of LNOx in chemistry and climate models is the significant variation in estimated LNOx production per flash (Pickerling et al., 2016). Estimates from various studies vary by 2 to 3 orders of magnitude (Biazar and McNider, 1995; Schumann and Huntrieser, 2007; Peterson and Beasley, 2011; Koshak 2014; Pickering et al., 2016). Some estimates are produced from post-discharge near field measurements around the storms with modeled dynamic and chemical processes (e.g., Franzblau & Popp, 1989; Barthe & Barth, 2008; Ott et al., 2010), deduced from columnar NOx of remotely sensed satellite observation (e.g. Miyazaki et al., 2014; Pickering et al., 2016; Zhu et al., 2019; Zhang et al., 2020), or constructed from theoretical or laboratory work (e.g. Price et al., 1997; Cooray et al., 2009). In a previous investigation, to improve LNOx estimates, a NASA Lightning Nitrogen Oxides Model (LNOM; Koshak et al., 2009; Koshak et al., 2010; Koshak et al., 2011; Koshak and Peterson, 2011; Koshak, 2014; Koshak, Peterson, et al., 2014) was developed that uniquely fused theoretical and laboratory results with ground-based Lightning Mapping Array (LMA) and National Lightning Detection Network^{TM} (NLDN) observations. The studies in Koshak, Peterson, et al. (2014), Koshak, Vant-Hull, et al. (2014), and Lapierre et al. (2020) showed that more LNOx was produced in cloud-to-ground (CG) flashes than in intra-cloud (IC) flashes. This is supported theoretically by the differences in the characteristic energy and path length between the two lightning types (Gallardo and Coory, 1996; Price et al., 1997). However, some studies report little difference between IC and CG NOx production (DeCaria et al., 2005; Barthe and Barth, 2008; Ott et al., 2010). Environmental factors such as the existence of ice crystals in IC flashes may reinforce cloud ice growth and, in turn, enhance LNOx production (Peterson and Beasley, 2011; Peterson and Hallett, 2012). Regional and seasonal differences can also sway the LNOx production estimates. Observations in mid-latitudes tend to report higher LNOx production per flash than those in the tropics (Schumann and Huntrieser, 2007). Despite all these uncertainties, Schumann and Huntrieser (2007) suggest a per-flash NO production of about 250 mol/flash for a global long-term average and <250 mol/flash for the trop-

ics. Some recent studies have used a value of 250 to 500 mol/flash in regional atmospheric transport modeling (Zhao et al., 2009; Allen et al., 2010; Ott et al., 2010; Zhu et al., 2019).

Previous studies attempting to assess the impact of LNOx on tropospheric chemistry have used different approaches for including LNOx emissions in chemical transport modeling. A common approach has been to include LNOx emission parameterization based on cloud-related variables (e.g. Deierling et al., 2008; Finney et al., 2014; 2016) or convection-related factors (e.g. Price et al., 1997; Allen and Pickering, 2002; Hansen, 2011; Romps, 2014). Koshak, Peterson, et al. (2014) used the observation-based LNOM to estimate LNOx for input to the Community Multiscale Air Quality (CMAQ) modeling system. With the LMA/NLDN combined lightning flash observations that provided details of the lightning channel (i.e., geometry, length, altitude, and CG peak current) and the laboratory/theoretical results that provided a way to parameterize flash-based LNOx production, the LNOM was able to give the vertical profiles of LNOx production for both CGs and ICs. The present approach in CMAQ is based on the NLDN observations (Allen et al., 2012; Kang et al, 2019a, b).

To attain broader geographical coverage and to capitalize on advances made in space-based lightning mapper instrumentation, Koshak, Vant-Hull, et al. (2014), Koshak (2017), and Koshak (2021) have introduced and applied methods for estimating LNOx production from individual lightning flashes. The first two studies by Koshak introduce what we refer to here as the "β-method". The β-method employs satellite-observed flash optical energetics to estimate flash LNOx production. As we will discuss in section 5.1, the β-method in Koshak (2017) represents an improvement to the β-method in Koshak, Peterson, et al. (2014) since it removes the effect of satellite orbit altitude changes that are important in the case of LNOx estimates from low Earth-orbiting (LEO) LIS data. The third study, called the *Virtual Capacitor Method (VCM)*, uses both the satellite-observed flash optical energy and flash optical area to estimate flash LNOx production (however, this more complicated method is not applied here but will be considered in the future pending additional analyses & comparisons with the β-method). Overall, these methods are ideally suited to benefit global and regional simulations of LNOx.

It is important to note that lightning has become a designated climate monitoring variable (Aich et al., 2018). The Geostationary Lightning Mapper (GLM) onboard the Geostationary Operational Environmental Satellite (GOES) R-series is the first to provide continuous and continental-scale lightning monitoring from space, leading the way to the formation of the international spaceborne lightning observation constellation (Rudlosky et al, 2019). Early assessments of the GLM performance (Koshak et al., 2018; Blakeslee et al., 2020; Murphy & Said, 2020; Zhang & Cummins, 2020) have shown that the overall GLM flash-level detection efficiency (DE) meets the pre-launch requirement of 70%, with better performance at night than during the day. In light of the recent work of Koshak, Vant-Hull, et al. (2014) and Koshak (2017; 2021), this may also be the

first step to providing continuous satellite-derived LNOx emissions to serve the climate and air quality communities.

Furthermore, assessments of air-quality/climate coupling as related to the influence of LNOx production on ozone concentration across the US, support the goals of the US Global Change Research Program's National Climate Assessment (NCA).

Hence, we have been motivated to initiate the development of a regional satellite-derived LNOx emissions model based on the methods in the previous work of Koshak, Peterson, et al., (2014), Koshak, Vant-Hull, et al. (2014), and Koshak (2017). This emission model may serve as an important prelude to a desired global emission model supported by the future satellite lightning observation constellation, and air pollution monitoring constellation, that are each underway.

In this study, we conduct a detailed evaluation of the relatively new GLM dataset to establish the robustness of observations for LNOx estimation. First, a total of 3-4 years of the latest GLM lightning observations are analyzed to obtain seasonal, geographical, and annual fluctuations within the GLM field of view (FOV). Second, GLM detection degradation with increasing view angle (and particularly near the edge of the FOV) is examined in order to devise ways to compensate for the degradation. Third, we use NLDN data to identify GLM-observed CG flashes so that we can inter-compare and contrast differences in GLM-observed CG and IC flash optical characteristics. The NLDN has a high CG flash detection efficiency, approximately in the 90-95% range over the contiguous US (CONUS); see Murphy et al. (2021) for a recent summary.

For the LNOx emission model, we briefly describe and discuss the method introduced in Koshak, Vant-Hull, et al. (2014) and Koshak (2017) that forms the backbone of our emission model. We apply the method to the GLM lightning observations over N. America for a preliminary evaluation. We also analyze lightning observations derived from the Lightning Imaging Sensor (LIS) onboard the low Earth-orbiting International Space Station (ISS) and apply the method to estimate LNOx emissions. We compare the results from GLM and ISS-LIS estimations to examine the efficacy of the method and demonstrate a path for using ISS-LIS observations to string together and cross-calibrate the regional LNOx estimates derived from the future global constellation of geostationary satellite lightning observations. Finally, using the ISS-LIS data and the method, we extend the Tropical Rainfall Measuring Mission (TRMM) LIS LNOx record derived in Koshak (2017).

For 3-D emissions, the model incorporates results from the GLM-NLDN matching and partly adapts the IC and CG flash properties from the NASA LNOM to generate LNOx production profiles.

GLM Lightning Observation

The GOES R-series comprise the newest generation of the GOES Satellites that includes R, S, T, and U in the series. The GOES-R was launched on November 19, 2016, and anchored at 89.5° W for testing and validation before moving to the GOES-East operational position as GOES-16 at 75.2° W in November 2017. GOES-16 started delivering data for research and weather monitoring after reaching provisional maturity in January 2018. Subsequently, GOES-17 was launched as GOES-S on March 1, 2018, reached provisional maturity in December 2018, and occupies the operational GOES-West position at 137.2°W. Most recently, the GOES-T satellite was launched on March 1, 2022; i.e. four years to the day after GOES-S. It is presently in the test check-out position, and will eventually be parked at 136.8°W as GOES-18 with a provisional maturity date scheduled (as of this writing) in late October of 2022.

Onboard these newest generation geostationary satellites reside the payload of GLM. Hereafter, we refer to the GLM onboard GOES-16 as GLM16, and the GLM onboard GOES-17 as GLM17. GLM16 is the first to provide continuous lightning observation from a geostationary satellite, covering the Americas and most of the Atlantic, and the eastern portion of the Pacific Ocean. GLM17 covers the central to the eastern Pacific Ocean, with N. America under its surveillance. The latitudinal coverage of the GLMs spans from 54° S to 54° N (Rudlosky et al., 2019). Their longitudinal coverage has a similar span, overlapping roughly between 130°W and 80°W, in the tropical to mid-latitude regions. Most of N. America is within the overlapped coverage. As mentioned above, the center longitudes of GLM16 and GLM17 are 75.2°W and 137.2°W, respectively. The two GOES satellites were built with a 10-year operational life expectancy. However, a cooling issue with the Advanced Baseline Imager (ABI) instrument on the GOES-17 is affecting measurements in the IR and near-IR channels. Biannual yaw flips of the spacecraft have been performed to lessen the thermal channel noise from the cooling issue (Sullivan 2020, Rudlosky and Virts, 2021). The yaw flips result in a slight shift of the GLM17 FOV to the east in cold months (roughly September to April) compared to that in the warm months (April to September) as shown in Figure 1 of Rudlosky and Virts (2021). Because of the issue with ABI, the plan is to replace GOES-17 operations with GOES-18.

The GLM is an optical charge-coupled device (CCD, a split frame-transfer device) imager that detects cloud-top lightning illumination at 777.4 nm within a 1-nm spectral bandwidth. The pixel footprint varies from 8 km at the nadir to 14 km at the limb (Rudlosky et al., 2019). The sensor captures lightning images at a frame rate of 500 frames/s, rendering a time resolution of 2 ms per frame. For our work in this study, we used the flash data from the quality-controlled GLM Level-2 product, which reports three lightning classes: *event*, *group*, and *flash*. An event is the fundamental pixel-level lightning optical detection. Adjacent (and diagonally touching) events in the same 2-ms frame are clustered into a group, which is further bundled with other neighboring groups within

designated spatial and temporal bounds to create a flash (for more information see Goodman et al., 2013). The Level-2 product also includes parameters such as detection time, optical energy, illuminated area, and identification numbers associated with these three classes and their relationship. Given the time tag on events, the flash duration can also be obtained from the Level-2 data. We used some of these parameters to represent the flash characteristics.

Since lightning varies greatly both seasonally and geographically, we analyzed nearly four years (March 2018 through December 2021) of GLM16 and nearly 3 years (February 2019 – December 2021) of GLM17 data. We utilized quality-controlled (Qflag = 0) data, and much of the data employed in our study contained important fixes as part of the NOAA/NASA Algorithm Discrepancy Report (ADR) and Work Request (WR) process. Note that these two periods also begin after each respective GLM reached provisional maturity; for more on the provisional maturity level see Marchand et al., (2019).

Distinctive seasonal patterns of lightning flash activity and per-flash energy are shown for both GLM16 and GLM17 in **Figure 1**. Lightning flash counts peak in the N. hemispheric summer months for the GLM17 full-disk coverage while the peak appears to be a few months lag for the GLM16 full-disk coverage (**Figure 1a**). The temporal lag can be explained by the geographical variation of lightning activity, as shown in **Figures 2 and 3a**. There is more lightning activity over land than over the ocean. Specifically, an early assessment of the GLM16 performance by Rudlosky et al. (2019) showed that 83% of the lightning activity was observed over land and only 17% over the ocean for the first three seasons of GLM16 observation. The temporal variation of lightning observed by GLM17 is dominated by lightning activity over the N. America continent. Lightning is most active in the summer (JJA) in N. America (**Figure 3a**). On the other hand, the GLM16 coverage includes the substantial landmass of the central and northern part of S. America in the tropical and sub-tropical areas that tilt the seasonal variation toward that of the northern hemisphere (**Figure 3a**).

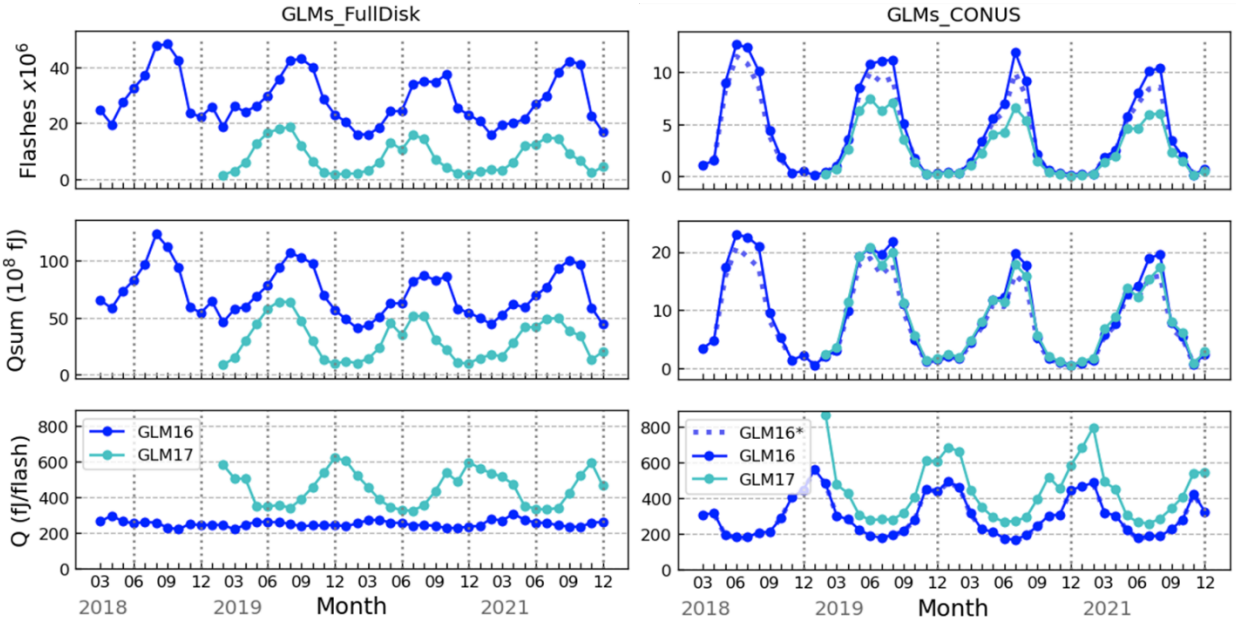

Figure 1. Time series of the monthly total lightning flash count, total lightning flash optical energy (Qsum), and lightning flash optical energy (Q) as observed by GLM16 (on GOES-East) and GLM17 (on GOES-West) for (a) the full disk and (b) CONUS. Note that GLM17 does not cover the east coast of CONUS. For a fair comparison to GLM17, GLM16* in (b) only counts GLM16 detected flashes in the overlapped GLM16/17 coverage in CONUS.

Note that the dotted line in **Figures 2** and **3** that shows the eastbound of the GLM17 FOV is for the warm months. Furthermore, the GLM17 data used for the analyses of the overlapped region in this paper is confined within the warm-month FOV eastbound so that the spatial coverage of the analyses does not vary with the time of the year.

One of the most distinctive features in **Figure 2** is the peak lightning activity over the Caribbean islands, as well as the link from southern Mexico through the Central America Land Bridge to northern Columbia; i.e. the maritime landmasses in the tropics. Peak lightning activity is also found in tropical S. America (the Amazon), but with lower frequencies compared to that in Central America.

While lightning activity is much higher over land than over the ocean, flash optical energy appears to be weaker over land, as shown in the bottom panels of **Figure 2**. The more energetic and brighter lightning over the ocean has also been documented previously from ground-based (Hutchins et al., 2013; Said et al., 2013; Cooray et al., 2014; Chronis et al., 2016) and satellite (Rudlosky & Shea, 2013; Beirle et al., 2014; Peterson et al., 2017; Rudlosky et al., 2019) observations. The weak lightning optical energy is most noticeable in extratropical

mid-land; i.e., the Great Plains to northern Mexico in N. America and the Plata River Basin in S. America.

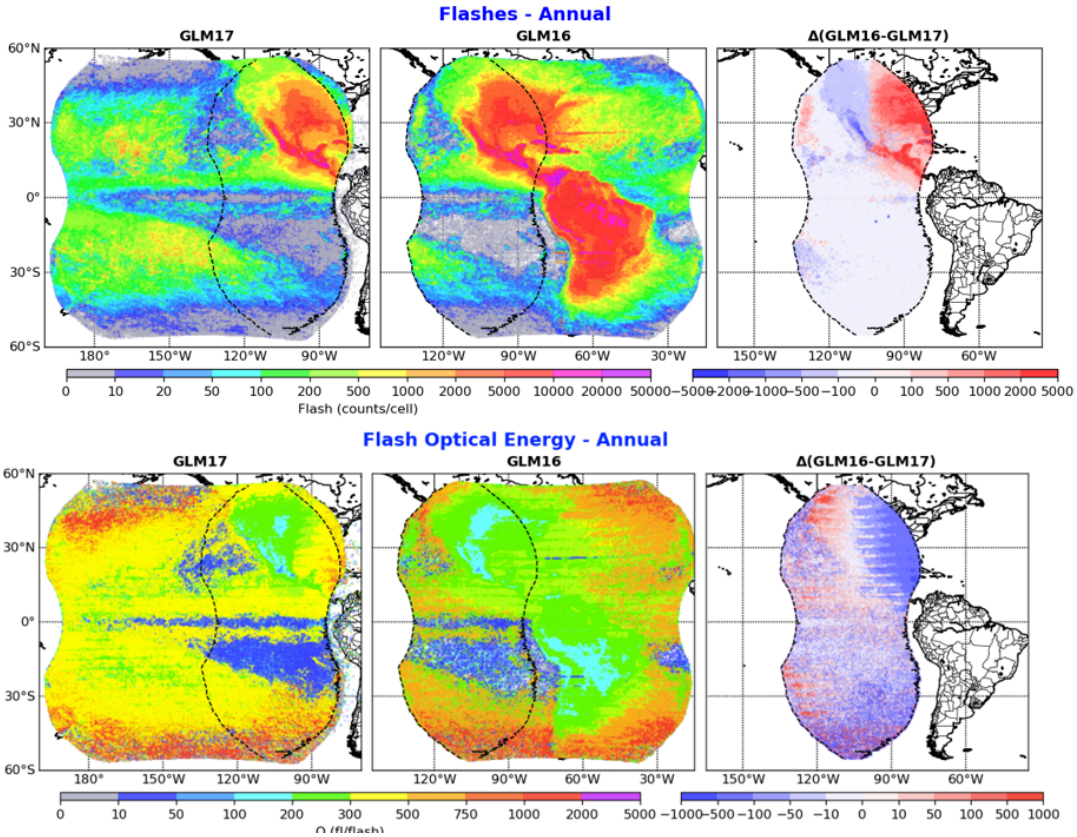

Figure 2. Mean annual geographical variation of total lightning flashes and flash optical energy Q per 0.2^0x0.2^0 cell as observed by GLM16 (on GOES-East) and GLM17 (on GOES-West) and the difference in overlapped coverage. The dotted line outlines the overlapped coverage area. Note that for a fair comparison, the observation period is taken from March 2019 through December 2021.

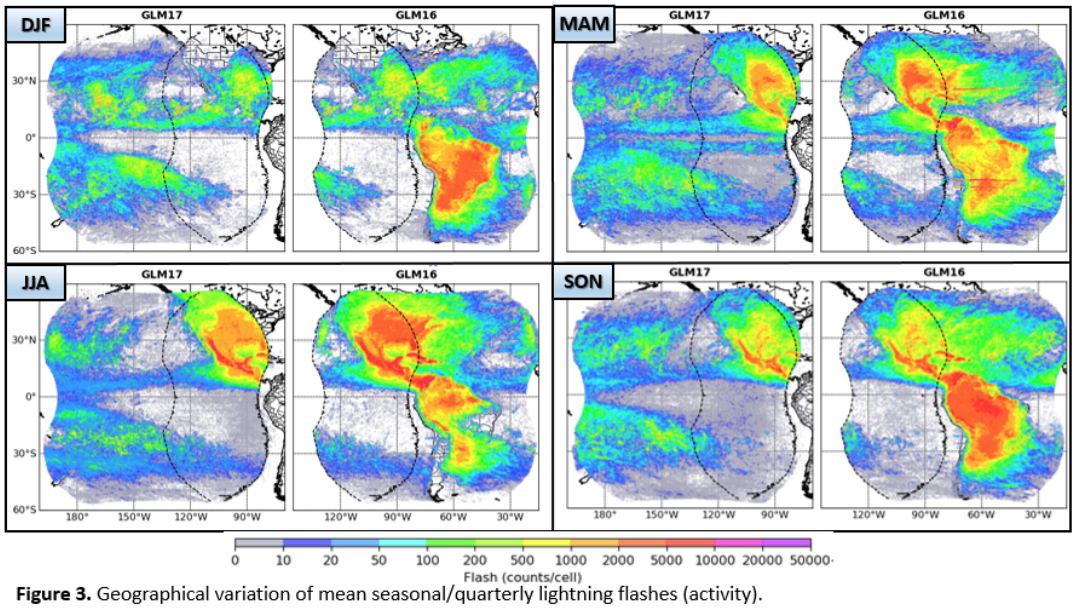

Figure 3. Geographical variation of mean seasonal/quarterly lightning flashes (activity).

Figure 3. Geographical variation of mean seasonal/quarterly lightning flash activity.

Moreover, the seasonal pattern of flash optical energy appears to be in the opposite phase with that of lightning activity for both GLM16/17 observations over CONUS and for GLM17 full-disk coverage (**Figure 1** bottom panels), as though lightning flashes in the prolific warm months are less energetic. However, the seasonal variation of flash optical energy for GLM16 full-disk is less apparent. The seasonal variation for GLM16 full-disk is only about 50 fJ/flash compared to $>$ 250 fJ/flash for GLM17. This lack of apparent seasonal pattern in GLM16 full-disk coverage may be the result of the compensation between the extratropical N. and S. hemispheres/Americas lightning with their respective most active months.

Overall, the mean monthly observations (**Table 1** and **Figure 4**) show peak lightning activity and lowest flash optical energy in June – August in GLM17 full-disk regions and in August – October in GLM16 full-disk regions. For CONUS, lightning activity takes off in May and stays elevated through August (**Table 1** and **Figure 4**). In the meantime, those months have the lowest flash optical energy. The inverse relationship between lightning activity and flash optical energy is consistent with the findings of Bruning and MacGorman (2013).

Table 1. Monthly mean of GLM observation of lighting flash count (Flashes), and optical energy per flash called "flash optical energy" (Q) over the period of (March 2018 through December 2021) for GLM16 and (February 2019 through December 2021) for GLM17, respectively. Note that Q refers to the optical energy measured at the satellite instruments. In addition, note that GLM17

does not cover the entire CONUS.

	Full Disk	CONUS						
month	GLM16 Flashes 10^6	GLM17 Q (fJ/flash)	GLM16 Flashes 10^6	GLM17 Q (fJ/flash)	Flashes 10^6	Q (fJ/flash)	Flashes 10^6	Q (fJ/flash)

Annual

Although the seasonal variation pattern repeats year after year, the annual fluctuation of the seasonal pattern is quite significant for lightning occurrences reflected by the flash counts in **Figures 4 and 5**. The difference of ~ 15x10^6 in monthly flash count in September between 2018 and 2020 of GLM16 detection is about 1/3 of the annual mean of ~45x10^6 for that month for the full-disk coverage. For the CONUS part, the largest difference of 5.7x10^6 comes in June, also between 2018 and 2020 of GLM16 detection and is larger than half (0.59) the annual mean of 9.64x10^6 for that month. Deviation of flash optical energy from the mean is rather small, especially for CONUS in the summer months. Among the 4 years of GLM lightning record, 2020 appears to be the least active year for CONUS (as well as the neighboring region from East Pacific through the Atlantic Ocean).

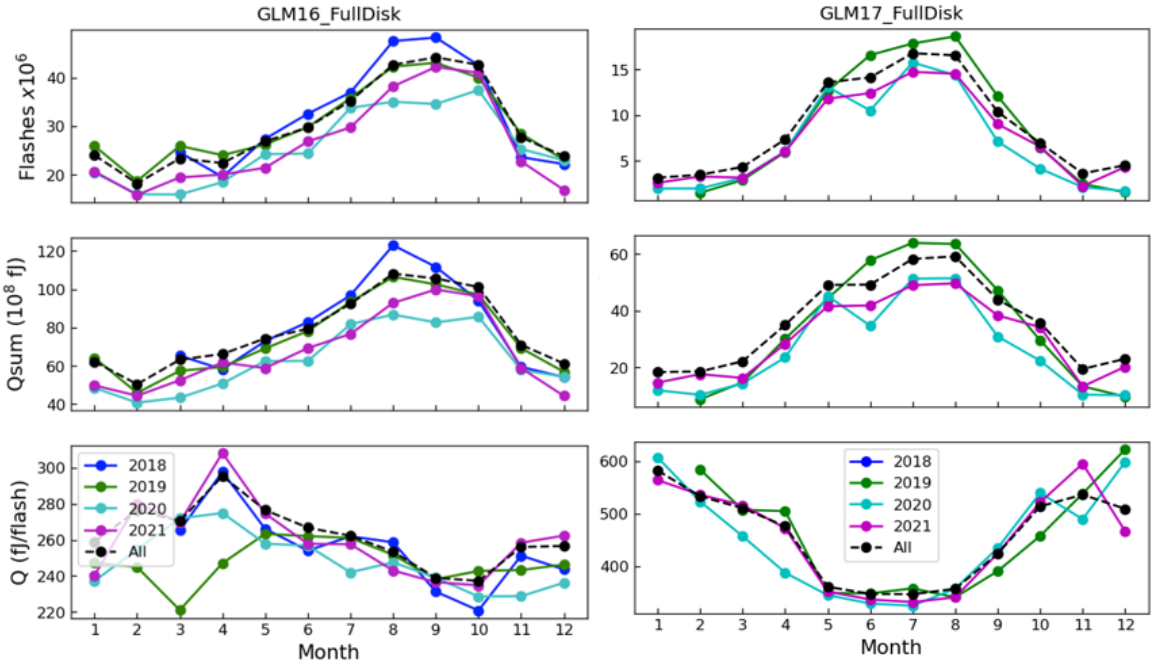

Figure 4. Mean and annual monthly variation of total lightning flash count, sum of lightning optical energy, and flash optical energy as observed by GLM16 (left panels) and GLM17 (right panels) for the full disk coverage.

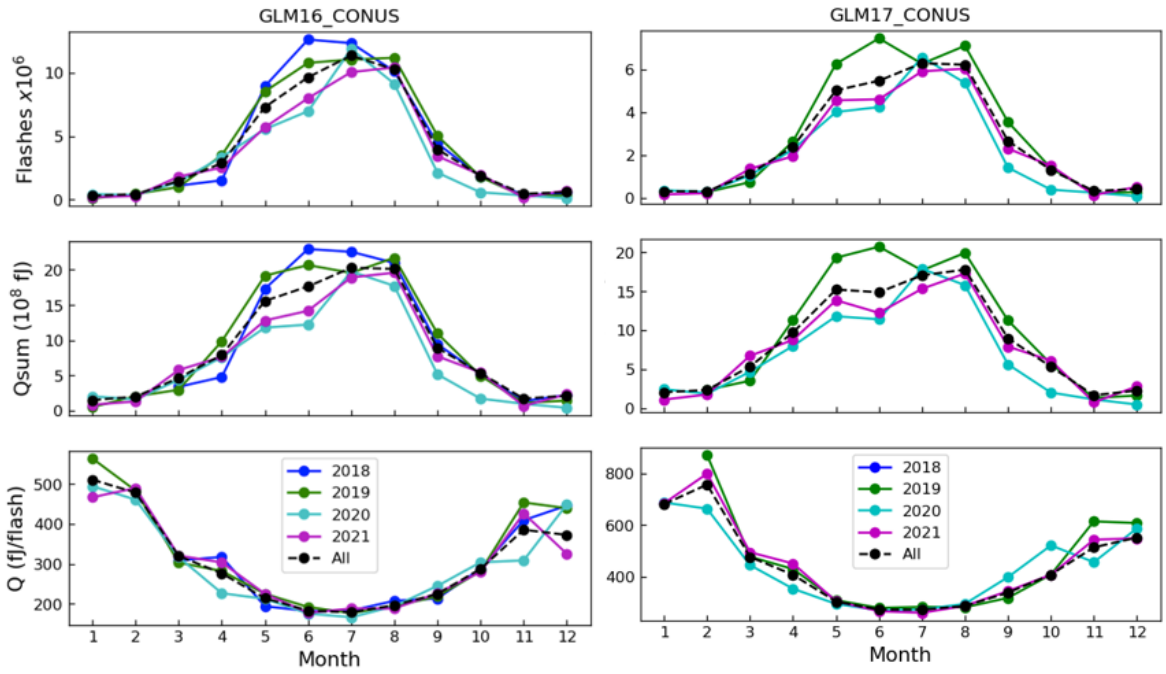

Figure 5. Same as **Figure 4**, but for CONUS coverage

Merging of GLM16 and GLM17

Koshak et al. (2018) evaluated the first 10-month of GLM16 performance (~240 million flashes) and showed an overall flash-level detection efficiency (DE) of 78% relative to combined ground-based networks, with 74% in the daytime and 82% at night. This assessment was in agreement with other studies that reported 68% to 74% of flash-level DE of GLM16 for local (Zhang & Cummins, 2020) or the overall coverage (Blakeslee et al., 2020; Murphy & Said, 2020). The assessed GLM false alarm rate was found to be <5% (Bateman & Mach, 2020). While the overall DE meets the pre-launch requirement of 70%, the DE shows geographical variation in addition to diurnal variation. Uneven spatial DE with low DE in some regions poses a challenge in applying the GLM data for LNOx emission estimates. GLM16 consistently shows a higher than 70% DE over the East CONUS (also over S. America and oceans), while the DE drops to 50-70% or below 50% toward the NW CONUS (Koshak et al., 2018; Marchand et al., 2019; Blakeslee et al., 2020; Murphy & Said, 2020). Similarly, the GLM17 DE was found to drop off toward its FOV edge over the CONUS (Murphy & Said, 2020).

Excluding likely quality artifacts (Rudlosky et al., 2019) near the edge of the GLM16/17 FOV overlap and the equator, there appear to be significant differences between lightning observations from GLM16 and 17 in the overlapped

coverage shown in **Figure 2**. The differences are most obvious and look systematic for both flash counts and flash optical energy over land, i.e. N. America. More lightning flashes are observed by GLM16 than 17 over the eastern part of the overlap, and vice versa over the western part. It points to a decline in the detection capability as the satellite viewing angle increases. This is in agreement with the previous assessments of the GLM performance that pointed to the diminished detection efficiency (<50%) of GLM16 in the NW US where (fortunately) lightning activity is far less. Murphy and Said (2020) indicated the DE started to decline within 2000 km of the FOV edge for both GLM16 and 17, particularly over land.

The decline of DE toward the FOV edge is the result of the spectral cut-off of the GLM filter near the FOV edge by design (private communication, NASA/NOAA's GOES-R series GLM engineering team). Nevertheless, it is of interest to identify the degree of the decline in detection capability and to find a way to compensate for the decline in order to optimize applications of the GLM observations.

Focusing on the difference in lightning flash counts and flash optical energy over the CONUS (land only), we analyzed nearly 3 years of GLM observations and found that the difference between GLM16 and 17 observations is quite symmetric; i.e., somewhat along the longitude line 106.2°W that sits in the middle of the GLM16 and 17 center longitudes (**Figures 6 a, b**). The GLM16 detected less lightning activity and recorded higher flash optical energy west of the longitude divide than the GLM17. The difference in flash counts does not seem to grow significantly to the west of 106.2°W. This is attributable in part to the decreasing lightning activity in the same direction. In the overlapped area over CONUS, both GLM16 and 17 observed more than 90% of flashes east of the divide. That leaves less than 10% of flashes observed west of the dividing longitude over the CONUS.

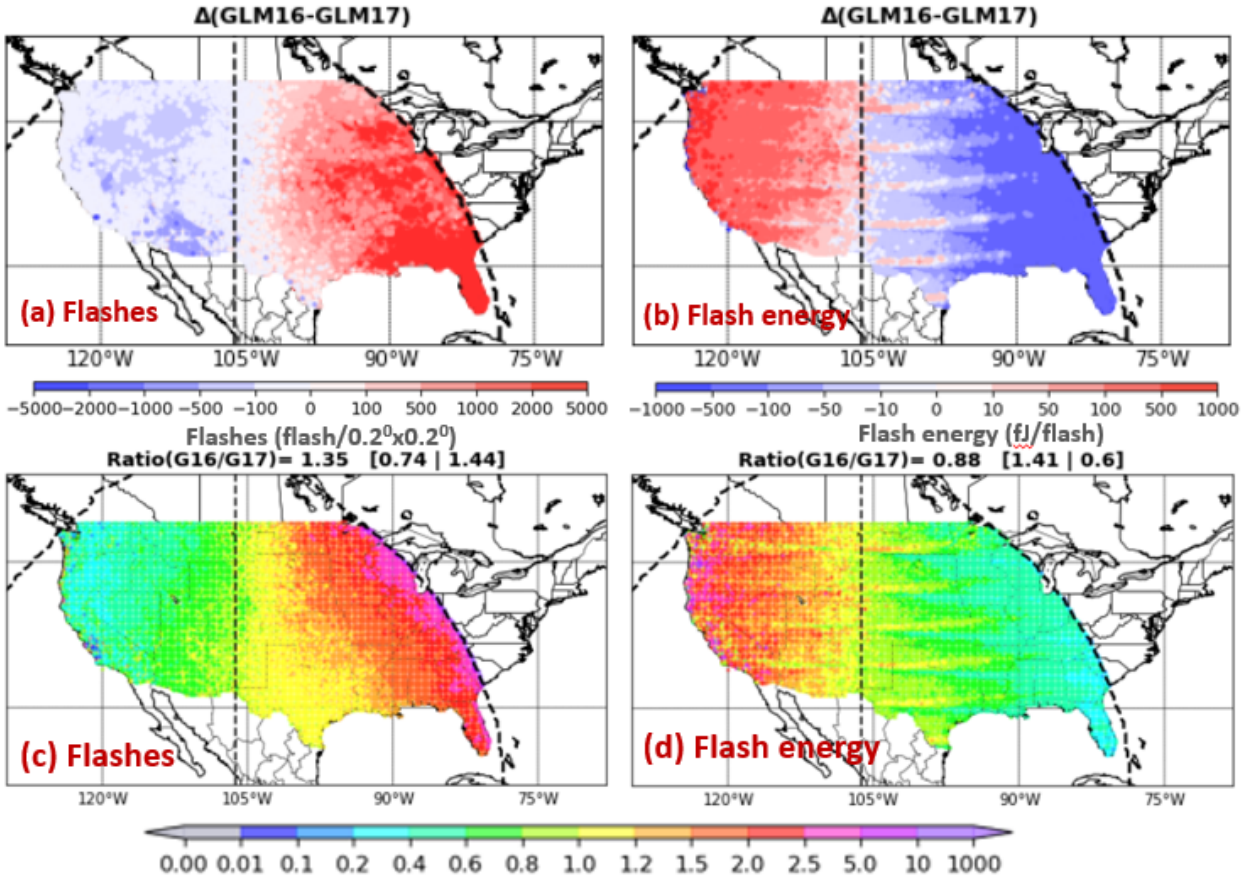

Figure 6. Difference between GLM16 and GLM17 observations in (a) flash count, (b) flash optical energy, and ratio of GLM16 to GLM17 observations in (c) flash count, (d) flash optical energy over CONUS. The vertical dashed line indicates 106.2 ^{0}W that is in the middle between the GLM16 and 17 center longitudes. The curved dashed lines show the confines of the overlapped GLM16 and 17 coverage. The three numbers in (c) and (d) title bar are the ratio for the overall, west, and east of the divide, respectively.

The ratio of GLM16 observation to that of GLM17 (**Figure 6 c,d**) demonstrates the detection edge degradation issue much more convincingly – moving from the east toward the west coast, the flash count ratio (GLM16/GLM17) decreases and the flash optical energy ratio increases. The ratios are ~ 1 around the 106.2°W longitude for both parameters. The GLM16/17 flash count ratio increases from 1 around the longitude divide to >3 near the eastbound of the overlapped coverage in **Figure 6**. It is just the opposite on the west of the divide, with the ratio dropping to < 0.2 on the west coast. On average, 44% (36%) more (less) flashes were observed by GLM16 than by GLM 17 over the east (west) of the divide. It is thus conceivable that both GLM16 and GLM17 have a similar and severe

degree of degradation as the viewing angle increases, especially when it gets close to the FOV edges. Based on this finding, we conclude that the use of GLM16 or GLM17 data alone or without correction for such degradation over these particular regions of CONUS should be avoided. Thus, for estimating LNOx production over CONUS from GLM flash optical energy observations, we combine both GLM16 and 17 data; we use GLM17 observations to the west of the dividing line and use GLM16 to the east of the dividing line.

In contrast to the degraded detection capability toward the FOV edges over land (i.e. N. America), the flash DE over the ocean is good across the board except at very close to the edges of the GLM coverage (Murphy and Said 2020). The DE over the ocean is shown to be quite high, above 80% on average, for both GLM16 and 17 in the assessments by Koshak. et al. (2018), Blakeslee et al. (2020), and Murphy and Said (2020). Thus, for applications using GLM observations over the ocean alone, the data merging can be done but is not necessary.

Another striking feature appearing in **Figure 6** is the horizontal striations in the flash optical energy plots (**6b** and **6d**). This is an artifact caused by radiometric calibration errors as the consequence of the non-linear response of the analog electrical readout in the GLM camera (private communication, NASA/NOAA's GOES-R series GLM engineering team). The GLM CCD is read out via 56 parallel output stripes to achieve a high frame rate (500 frames/s). Due to design considerations, 4 dark pixels are added to each subarray, causing a non-linear ringing behavior in the analog voltage waveform representing each pixel. This ringing or overshoot behavior is particularly pronounced on contrast edges at the boundary between subarrays and is most apparent at the northern (southern) edge of the readout stripes in the N. (S.) hemisphere. Currently, we have not come up with a method to effectively remove the striations. This is on the list of our future plans to improve for applications using the flash/group/event optical energy product.

We made a composite of the blended GLM16 and 17 observations based on the aforementioned principle to show the geographical distribution of lightning activity, per annual mean overall, diurnal, and seasonal variation over the CONUS for the nearly 3 year-period from February 2019 through December 2021 (**Figure 7**). Overall, most lightning activity happens in the eastern US, excluding the NE states, with an overwhelming 94% of lightning flashes occurring east of the Rockies. The most active of all are in Florida. For the diurnal variation, we see an interesting geographical contrast: lightning is more active in the SE coastal states (most active in Florida) during the day and in the Central Plains at night.

Seasonally, the winter (DJF) has the lowest lightning activity, with occurrences limited to the southern states, mostly from eastern Texas to western Alabama. Florida does not see much lightning during this cold season. The lightning activity takes off in the south and spreads further inland and over Florida in the springtime (MAM) and extends to most of East US and the Central Plain (except the Northeast and southern Texas) during the summer months (JJA),

before greatly reduced activity in the fall (SON). Two-thirds (28.84/43.22 = 0.67) of the overall lightning occurrences happen in the summer months (JJA) alone, suggesting a potentially large impact of LNOx in the summer months in the US.

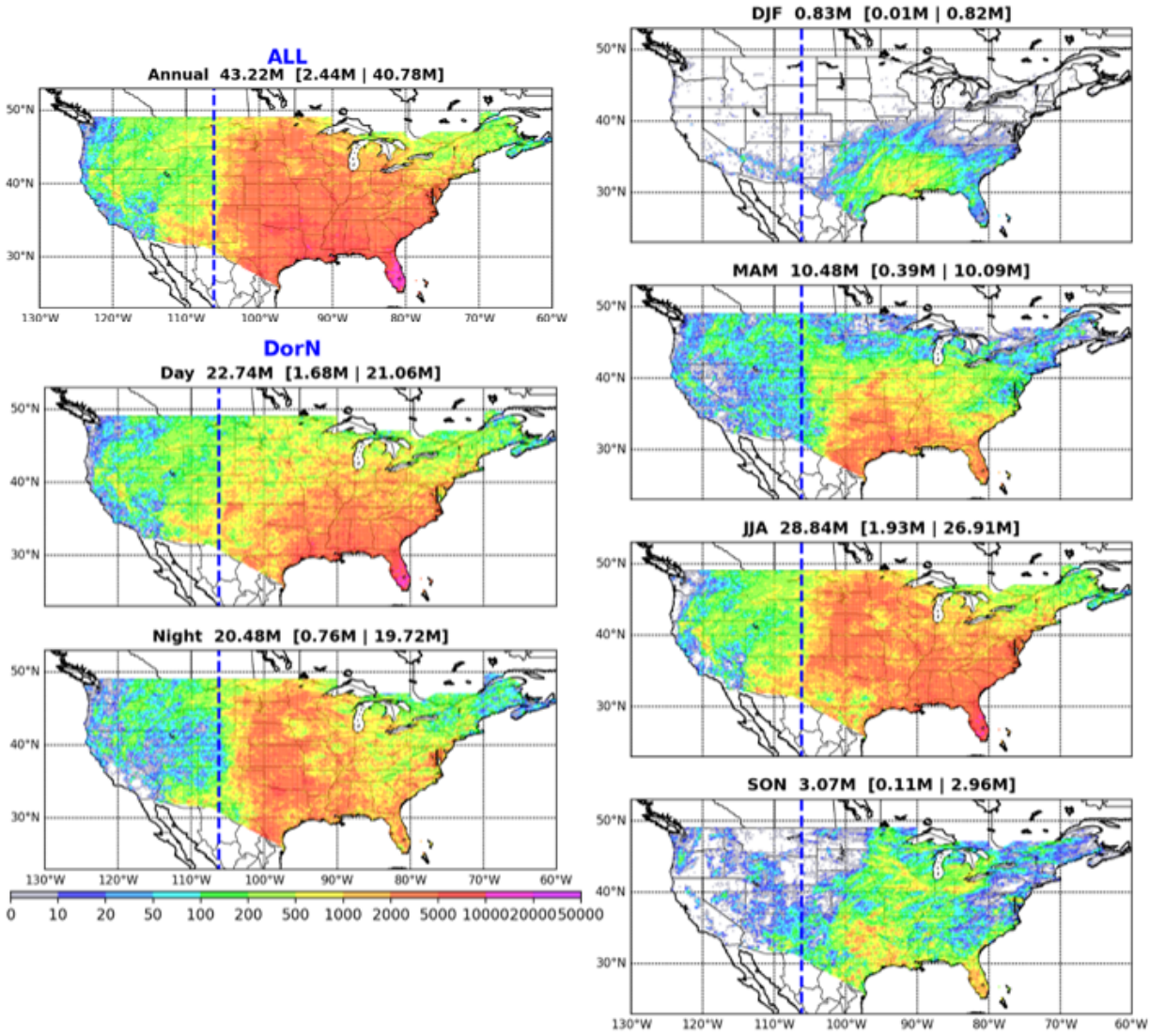

Figure 7. Geographical variation of annual mean (a) overall, (b)-(c) diurnal, (d)-(g) seasonal lightning flashes over CONUS from GLM observation compiled for the period of March 2019 through December 2021. GLM16/17 data are used east/west of 106.2^0W.

Matching GLM – NLDN Flashes

A substantial number of previous studies use the per-flash NOx production rate to quantify the total annual contribution of LNOx to the global NOx budget. In fact, this extrapolation is used as a constraint to justify the credibility of per flash estimates. However, global LNOx estimates use many tunable parameters that can contribute to the uncertainties in the per-flash estimates. One of these parameters is the IC/CG ratio and NOx (or NO) production from IC versus CG flashes.

An additional factor related to this issue is the estimations being stroke-based or flash-based. An IC flash is composed of one or more IC strokes, while a CG flash consists of one or more CG strokes (and may also contain IC strokes). Since a flash may contain one or multiple strokes and a CG flash may include IC stroke(s), a stroke-based estimation not only can be very different from a flash-based estimation, the estimation ratio of IC-to-CG will be different for the stroke- and flash-based approaches, in general. Factors such as flash length, flash duration, and peak current also can contribute to the large uncertainties of the LNOx production estimates. Since LNOx is produced by the intense heating of the air from a lightning discharge, it is expected that a lightning flash with a longer length or larger peak current (i.e., with larger net energy) would lead to more LNOx production. Indeed, there were studies that showed CG flashes have substantially higher peak current, flash length, and areal extent (Rakov & Uman, 2003; Koshak, et al., 2010; Koshak, 2014). However, some studies found indifference in lightning energy and/or LNOx production from IC or CG discharges (e.g. Gallardo & Cooray, 1996; Cooray et al., 2009; Barthe & Barth, 2008; Ott et al., 2010). Recently, Lapierre et al. (2020) obtained results that show CG strokes may produce ~10 times more NO_2 than IC strokes. In an attempt to determine GLM DE, Zhang and Cummins (2020) showed that CG flashes tend to have greater energy and areal extent compared to IC flashes and that this may be the reason CG flashes are more likely to be detected than IC flashes by the GLM.

Hence, to fully understand LNOx production, it is beneficial to be cognizant of the ratio of the IC flash count to the CG flash count (i.e., the so-called "Z-ratio"). For example, the value of Z directly affects the vertical distribution of LNOx within a column. Thus, here we attempt to ascertain information about the characteristics of CG flash count versus IC flash count in GLM observations. In their study, Zhang and Cummins (2020) referred to any LIS flash that was associated with an NLDN observed CG flash (NLDN-CG hereafter) in time and space as a LIS CG flash and the un-associated flashes as LIS IC flashes. Similarly, we took advantage of the high DE (90-95%) of the NLDN-CG in the CONUS network and tried to match and associate the GLM flashes with the NLDN-CG.

We used NLDN-CG and GLM detected flashes for the entire year of 2020 over the CONUS. It should be noted that GLM and NLDN observe different properties

of lightning: optical radiance from cloud top for GLM versus electromagnetic current (peak current) of a lightning stroke/pulse for NLDN. The GLM has a pixel footprint of 8-14 km from the nadir to the FOV edge while the NLDN network locates a lightning stroke/pulse at an accuracy of 200-300 m (Nag et al., 2014). There is no guarantee that a GLM-detected discharge is equivalent to an NLDN-detected discharge given the shear pixel size of GLM, the differences between optical and VLF/LF radio emissions, and the fact that the optical emission is cloud-scattered but the VLF/LF radio emission is not.

At the flash level, a GLM flash is a cluster of groups that each is composed of neighboring events in the same individual 2 ms timeframe. The GLM clustering algorithm (Mach, 2020) has groups within 330 ms and 16.5 km of each other assembled into a flash. The cut-off time for a GLM flash duration is 3 s while no limit is set for the spatial extent, and the recorded flash location is the centroid of the groups in the flash. In contrast, the NLDN clustering algorithm (Murphy et al., 2021) groups detected CG/IC strokes/pulses within 10/20 km from the first stroke and 500 ms of a previously added stroke into a flash. The maximum duration and extent of an NLDN-CG flash are 1 s and 10 km, respectively. The recorded flash location is that of the first return stroke. Taken into account also is the GLM's geolocation error that grows to 20-30 km near the GLM FOV edge (Virts and Koshak, 2020). Considering all these incongruences, the criteria for NLDN-to-GLM matching used in this study include a distance of 50 km and a temporal window of 1 s before and 3 s after a GLM flash, and multiple NLDN-CG flashes are allowed to be matched to a GLM flash.

The matching criteria employed in this study are different from those used in studies focused on validating/assessing GLM DE (Bateman & Mach, 2020; Blakeslee et al. 2020; Murphy & Said 2020; Zhang & Cummins 2020). Previous studies, such as Zhang and Cummins (2020), used the GLM-group/NLDN-stroke level data that are more suitable for DE assessment that can be used to mitigate the inconsistencies in flash clustering and centroid definition. Our primary goal is to obtain characteristics of GLM-observed CG flashes and help ascertain GLM's detection capability. The matching results give higher matched percentages than the DEs obtained from previous assessments in Koshak et al. (2018), Blakeslee et al. (2020), and Murphy & Said (2020) as the criteria windows we used are wider. Note that Bateman et al. (2021) widened the matching time window to 10 min and obtained DE of over 90% for both GLM16 and 17. Our results show an overall good agreement with these previous DE assessments in geographical variation. The results presented in **Table 2** and **Figure 8** show that:

- overall, ~ 86.5% (74.6 %) of NLDN-CG flashes are matched to GLM16 (17) flashes;
- the matching percentage declines toward the edge of FOV;
- both GLM16 and 17 show a lower matching percentage around 106.2°W;
- comparing the results, the percentage of NLDN-CG flashes matched to

GLM16 (87.7 %) is substantially higher than to GLM17 (74.8 %) east of 106.2° W;

- percentage of NLDN-CG flashes matched to GLM16 (57.6 %) is substantially lower than to GLM17 (69.4 %) west of the divide longitude; and
- roughly, 96 (90) % of flashes detected by GLM16 (17) are located east of the 106.2° W longitude line.

Table 2. GLM observed flashes and percentage of NLDN CG flashes matched to the GLM flashes over CONUS in 2020. West/East refers to west/east of the 106.2^0W longitude. GLM16* include flashes only within the GLM17 FOV eastern bound.

	GLM16	GLM16*	GLM17						
	All	West	**East**	All	West	**East**	All	**West**	East
Flashes (10^6)	42.09	1.74	**40.41**	36.78	1.74	**35.04**	26.17	**2.52**	23.71
Annual (%)	86.5	57.6	**87.7**	86.3	57.6	**87.7**	74.6	**69.4**	74.8
Day (%)	83.0	53.2	**84.7**	82.5	53.2	**84.4**	67.0	**65.1**	67.1
Night (%)	90.4	67.3	**91.0**	90.4	67.3	**91.1**	82.6	**79.2**	82.7

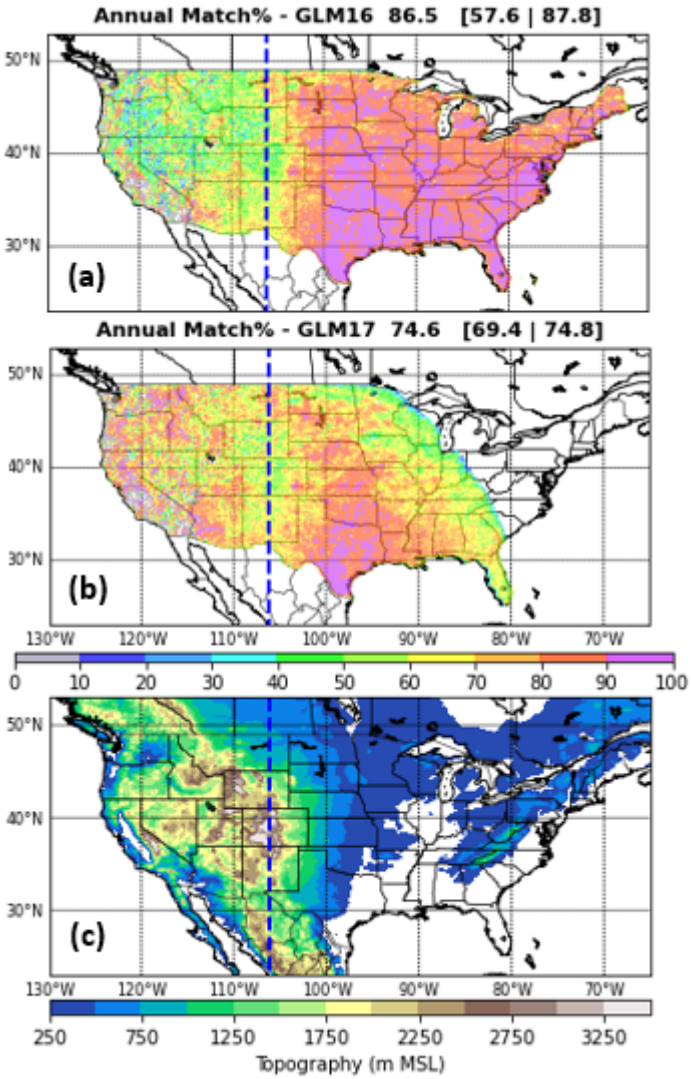

Figure 8. Matching NLDN-CG flashes to GLM flashes, percentage of NLDN-CG flashes matched to flashes detected by (a) GLM16 and (b) GLM17; (c) topography of the N. America. The vertical dashed line indicates the 106.2 ^{0}W longitude. The three numbers in the title bars of (a) and (b) are the matching percentage for the overall, west, and east of the longitude divide, respectively.

The overall lower matching percentage for GLM17 simply reflects the heavy weighting from the east side, which is close to the FOV edge of GLM17. After all, the ratio of (matched to GLM17)/(matched to GLM16) = 69.4/57.6 ~ 1.20 over the west of the dividing longitude is comparable to that of (matched to GLM16)/(matched to GLM17) ratio of 87.7/74.6 ~ 1.18 over the east of the

dividing longitude.

The depressed matching percentage (50 – 60 %) around 106.2 ^{0}W (**Figure 8 a, b**) might be caused by detection degradation toward the FOV edge for both GLM16/17 (Murphy and Said, 2020), reduced GLM DE over high lands, and/or more lightning activity in this area occurring during the day (**Figure 6**) when GLM DE is also reduced. Decreased GLM DE has also been shown over high altitudes during daytime in S. America (Figure 4 in Murphy and Said, 2020). We note that both Marchand et al. (2019) and Rutledge et al. (2020) have reported low GLM16 DE over the western Great Plains. These studies are more focused on the IC flashes and low DE attributable to inverted IC polarity and related deep convection cloud morphology in scattering the lightning optical energy.

For overall GLM flash characteristics (**Table 3**), an average flash observed by GLM16/17 lasted 280/250 ms, extended 337/282 km^2, and emitted 203/315 fJ (received at GLM sensors). These numbers are in line with those obtained by Rudlosky et al (2018). For the flashes matched to NLDN-CGs, an average flash lasted longer (343/300 ms), extended farther out (504/378 km^2), and was brighter (333/522 fJ) than the unmatched (263/233 ms, 293/249 km^2, 168/196 fJ) for GLM16/17. Assuming those matched to NLDN-CG flashes are indeed CG flashes and the unmatched ones are comprised mostly of IC flashes, we would obtain a CG/IC ratio of ~0.3 (0.27 – 0.34). The matching results suggest that on average CG flashes may last 30% longer, stretch out 50-70% more, and be more than 100% brighter than the IC flashes as illustrated in **Table 3** for the matched/unmatched ratios. These numbers are likely to be in the lower end since GLM's detection of IC flashes likely is much less efficient compared to that of CG flashes based on the assessment in Zhang and Cummins (2020). Undetected flashes tend to have short durations and/or are less energetic (below detection limit). Obviously, more IC flashes could fall into this category.

Table 3. GLM flash mean characteristics. Flashes are the total flash counts over CONUS. Flash duration (Tdur), flash optical energy (Q), and flash area (Area) are the mean values. "Matched" are for the flashes with NLDN-CG matches, and "Unmatched" (or "Unmat") are those cannot find an NLDN-CG match.

	All	Matched	Unmatched	**Mat/Unmat**				
	GLM16	GLM16*	GLM17	GLM16	GLM16*	GLM17	GLM16	GLM16*
Flashes (10^6)	42.09	36.73	26.17	8.95	8.00	6.61	33.14	28.73
Tdur (ms)	280	281	250	343	343	300	263	264
Q (fJ)	203	200	315	333	323	522	168	166
Area (km2)	338	337	282	504	495	378	293	293

Overall there are significant differences, and matched flashes (likely to be CG) tend to be twice as energetic (brighter) on average, the differences are not quite

as large as an order of magnitude. Additional insight (using GLM16 observations over CONUS) is provided in Koshak (2021) where again, the CG flash energetics significantly exceed the IC flash energetics, and winter-time flash energetics exceed summer-time flash energetics.

Satellite-Derived LNOx Emission Modeling

5.1 Overview of the -Method

In this section, we summarize the β-method introduced in Koshak, Vant-Hull, et al. (2014) and Koshak (2017) for estimating LNOx from LIS- and GLM-observed flash optical energetics. The -method is what we will apply in the current study to estimate LNOx from the ISS-LIS and GLM.

The -method introduced in Koshak, Vant-Hull, et al. (2014) was intended for low Earth-orbiting LIS data applications. The LIS Level-2 flash "energy" data product is actually a spectral energy density $_k$ (i.e. a time-integrated radiance) in units of J/m^2/sr/nm for the k^{th} observed flash. Therefore, to obtain the flash energy Q_k (typically represented in units of femtoJoules, fJ = 10^{-15} J) for a particular k^{th} observed flash one simply integrates the spectral energy density over the instrument entrance pupil area A (square meters, m^2), the flash solid angle Ω_k (in steradians, sr), and the instrument spectral bandpass Δ (in nanometers, nm). By contrast, the GLM Level-2 data directly provides the flash energy in Joules, so the value of Q_k is obtained directly.

The basic idea behind the -method is to assume that the satellite lightning mapper measures a very tiny fraction ($_k$) of the total flash energy E_k (typically in gigajoules, GJ); i.e., $Q_k =$ $_k$ E_k. This implies that $_k = Q_k/E_k$. For GLM, the magnitude of Q_k is typically hundreds of fJ, and E_k is on the order of a GJ, so the expected magnitude of $_k$ is on the order of 10^{-13} J/ 10^9 J ~ 10^{-22} which is indeed a very tiny fraction. In other words, the narrow-band (~ 1 nm) satellite lightning mapper intercepts only a tiny portion of diffuse, cloud-scattered optical energy from a lightning flash that, overall, has tremendous amounts of energy that is radiated in all directions in both the acoustical and across the electromagnetic spectrum. Finally, to estimate LNOx production P_k from the flash, one converts the flash energy to moles; i.e. $P_k = (Y/N_{\text{A}})E_k$, where is the thermo-chemical yield of NOx (~10^{17} molecules/J), and is Avogadro's number (6.022×10^{23} molecules/mol). As discussed in Koshak, Vant-Hull, et al. (2014), the value of $_k$ depends on the instrument characteristics (e.g., orbit altitude, bandwidth, entrance pupil diameter, …) and also varies with changes in nature (i.e., cloud scattering properties and lightning source properties). For a large sample of N flashes detected by a given satellite lightning mapper across a myriad of geographical regions and cloud morphologies, it was assumed that a fixed (mean) value for $_k$ could be used; i.e. $_k \sim$ so that the total LNOx production P from the N flashes can be obtained as follows

$$P = N\overline{P} = \sum_{k=1}^{N} P_k = \sum_{k=1}^{N} \frac{Y}{N_A} E_k = \frac{Y}{\text{N}_A} \sum_{k=1}^{N} Q_k \ , \quad (1)$$

where $\overline{P}$ is the mean LNOx production per flash of the N detected flashes. To obtain the value of , Koshak, Vant-Hull, et al. (2014) introduced a novel calibration technique wherein a reference year of data was examined containing a very large value of N flashes. For the reference year, the mean LNOx production per flash $\overline{P}$ was assigned a reasonable value cited in the literature; i.e., 250 NO mol/flash from Schumann and Huntrieser (2007). Note that in regional chemical transport modeling, $\overline{P}$ is often assumed to be ~250 or 500 mol/flash (Zhao et al., 2009; Allen et al., 2010; Ott et al., 2010; Zhu et al., 2019). With the known values of N, Y, N_A, and the assumed value $\overline{P}$ = 250 mol/flash, equation (1) is then solved for . With found in this way, the last expression on the right in (1) can be used to find the LNOx production P in a new set of N flashes. In effect, the value of is linked to the assumed average production rate $\overline{P}$, so that the LNOx production from each individual flash is determined by the flash energy while the total global (and/or regional) nitrogen budget is still constrained by the choice of $\overline{P}$.

As a side-note regarding the computation of Q_k, Koshak, Vant-Hull, et al. (2014) employed the LIS entrance aperture area A' instead of the (technically correct) entrance pupil area A, because that is all the author had available at the time (and because the area used does not affect the LNOx production value). That is, since $A' > A$, this means that flash optical energies were technically overestimated [i.e., $Q'_k = (A'/A)Q_k$] and thus the value of the reference beta was also overestimated [i.e. $' = (A'/A)$]. But this does not matter because it has no effect on the LNOx production; i.e. substituting these expressions into (1) gives $P' = P$. So note that the value 1.8675 x 10^{-19} provided in Koshak, Vant-Hull, et al. (2014) is the value $'$.

The Koshak, Vant-Hull, et al. (2014) -method given in (1) can be applied directly to GLM flash optical energy data (and as we mentioned above, GLM provides the Q_k values directly). Because GLM is at a higher (geostationary) orbit altitude and because its entrance pupil diameter differs from LIS, the values of Q_k, $_k$, and all differ from that obtained for LIS.

Because flash optical energy amplitude falls off with a $1/z^2$ dependence, where z is the satellite orbital altitude, changes in orbital altitude can bias/complicate flash LNOx retrievals provided by the standard -method given in (1). By taking the vertical mathematical derivative of the $1/z^2$ dependence, one gets a $1/z^3$ dependence, which indicates that the rate of change in the values of Q_k with changes in z is most pronounced/significant at lower orbit altitudes. This means that changes in the GLM altitude can be neglected (i.e., application of the standard -method given in (1) is reasonable, given the very high and stable geosynchronous orbit altitude). However, the changes in orbit altitude that occurred with the TRMM/LIS (including an orbital boost from about 350 km to 402 km), and the routine variations in the ISS/LIS orbit altitude motivate a desire to remove this bias.

Therefore, Koshak (2017) introduced a way to remove the orbital altitude bias. Instead of using LIS spectral energy density to obtain the flash optical energy

Q_k intercepted at the LIS instrument altitude, Koshak made a novel adjustment by instead computing the total upward optical flux *from the cloud-top surface,* a quantity that is independent of instrument altitude. This involves integrating over flash-illuminated pixel footprint areas rather than integrating over the LIS entrance pupil area, and pixel solid angles. In computing the upward optical flux, Koshak assumed that the diffuse cloud-top lightning optical emission was isotropic with spectral energy density $_k$ (which varies both in space and time; i.e. across the different instrument pixels and frame-times occupied by the flash). That is, for a given set of flash-illuminated pixel footprints in a particular 2 ms instrument frame, an (assumed isotropic) cloud-top spectral energy density emission is available to sum up in the process of finding the net upward optical energy from cloud-top due to the flash. Because this total upward optical flux F_k is evaluated at the cloud-top and incorporates the diffuse emission from the entire upper 2 steradians it is a far larger value than Q_k , and is derived in Koshak (2017) as,

$F_k = \sum_{i=1}^{m} \sum_{j=1}^{n} (\pi a_j \, \xi_{\mathrm{ij}}) \Delta\lambda$ (2)

where a_j is the pixel footprint, and the flash illuminates a total of n pixels across m frames. So in this orbit-independent -method, the fraction of total flash energy is now given by $_k = F_k / E_k$, and this fraction is larger than before since $F_k > Q_k$. The same calibration technique and approach for getting the LNOx production P is done as described using (1), but with Q_k replaced with F_k [see Koshak (2017) for additional details].

Applying -Method to GLM Data (Regional LNOx Emissions Modeling)

For a CMAQ simulation with the domain covering N. America that includes CONUS, part of Canada and Mexico, and adjacent waters, we processed nearly 3 years (February 2019 through December 2021) of GLM16 and 17 data to obtain N $\overline{P}$ and estimated $= 1.5336\text{x}10^{-22}$. Subsequently, with this value, we calculated annual LNOx production P estimates of 12.57, 9.35, and 10.61 $\text{x}10^9$ moles over CONUS for 2019 (Feb-Dec), 2020, and 2021, respectively. Seasonally, we obtained 0.71, 4.0, 8.06, and 1.95 $\text{x}10^9$ moles for the DJF, MAM, JJA, and SON for the CONUS, respectively. That gives the summer (winter) months 55% (<5%) of the annual P share. The seasonal per flash averages show an opposite trend. For these 3 years, they are 468, 265, 197, and 267 mol/flash for DJF, MAM, JJA, and SON, respectively, with the summer lowest values of about 75-100 mol/flash located in the northern Great Plain (**Figure 9**). The average summer (JJA) per flash value (**Figure 9**) is considerably high (~ 200 mol/flash) compared with the recent estimates from Pickering et al. (2016) and Zhang et al. (2020) (referred to as "PZ" hereafter) for the Gulf of Mexico coast in the summertime. These two recent estimates (80 ± 45 and 90 ± 50 mol NOx/flash) from PZ are retrieved from the Ozone Monitoring Instrument (OMI) NO_2 observations with simulated parameterized NOx emissions of ground-based lightning observation. These results are in contrast with other studies suggest-

ing a larger per flash production rate of up to 500 mol/flash (Kang et al., 2020; Zhao et al., 2009; Allen et al., 2010; Ott et al., 2010; Zhu et al., 2019) and present a lower range of estimates. Regardless of the uncertainties involved in the parameterization and simulation processes in PZ, two factors should be taken into account when comparing our estimates with those such as PZ's: 1) the GLM flashes may not directly correspond to flashes from the ground-based measurements. As outlined in the NLDN-GLM comparison section, different measurements and clustering algorithms define a flash differently. This is manifested by the fact that 13-17% of the matched GLM flashes were associated with multiple NLDN-CG flashes based on the results of our NLDN-GLM matching. Thus, on average, the per flash values obtained from our model likely will be higher compared to the values based on NLDN flashes; 2) the -value used in our study is based on the grand overall average $\overline{P} = 250$ mol/flash for the regional domain. It is obvious that these two factors are specific to the satellite dataset.

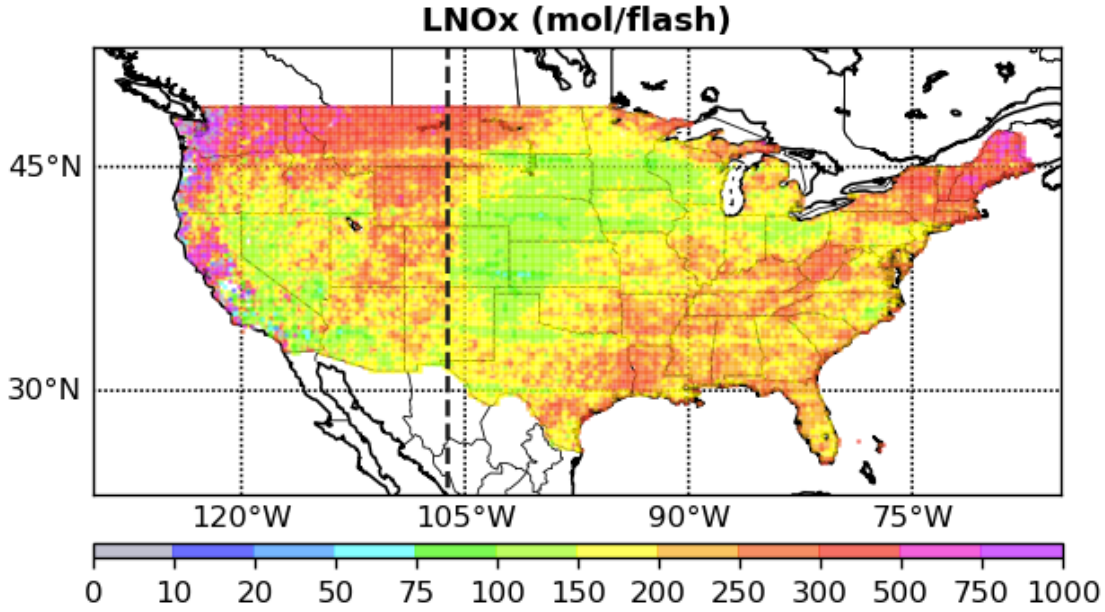

Figure 9. Averaged LNOx per flash in mol/flash in JJA months estimated from three years (2019-2021) of GLM observation.

The value of used in our GLM data analysis can be further fine-tuned or verified by comparing with NOx production from associated NOx or NO_2 observations and model simulation. Indeed, the preliminary results from an accompanying air quality modeling study for the summer of 2019 over the N. America show that the satellite-derived estimates from our technique account for about 12% of the total NOx emissions (personal communication). This is comparable but less than the estimates from other techniques. Zhang et al. (2003) used NLDN CG flash observations to estimate LNOx emissions. They reported that LNOx

contribution accounted for 14% of total NOx emissions in July. However, based on the trace gas evaluation for the 2019 study it seems that there is a need to revise the scaling factor to increase our LNOx estimates. This means increasing the average 250 NO mol/flash production rate used in our calculation of .

Furthermore, the Tropospheric Emissions: Monitoring Pollution (TEMPO) instrument scheduled to be launched in 2022 onboard a geostationary satellite will provide an excellent opportunity to verify and further constrain our value by comparing the CMAQ simulation results of predicted NOx production with the TEMPO observed NO_2. The TEMPO, expected to anchor at 100^0W and 36.5^0N, measures columnar NO_2, among a few other chemical species and aerosols and cloud properties at a resolution of 2 km/pixel in the N-S direction and 4.5 km/pixel in the E-W direction at the center of the field-of-regard. It will provide observations of the chemical and aerosol species similar to OMI, but at a much finer resolution under continuous monitoring.

Applying -Method to ISS-LIS Data (Extending the Long-Term LNOx Record)

For data from the LIS, onboard the TRMM satellite, Koshak (2017) obtained $= 3.94\text{x}10^{-11}$ by assuming $\overline{P} = 250$ mol/flash over CONUS for an arbitrarily selected reference year (1998); this value of is based on the upward optical flux F_k discussed above in (2). With this value, Koshak (2017) estimated the annual LNOx over the CONUS for 17 full years (1998-2014) of TRMM-LIS observation (shown in the green line in **Figure 10)**. Keep in mind that LIS is on the low earth-orbiting TRMM (or ISS) and has a short viewing time of 80 to 90 s at any location with a FOV of about 600km x 600km. It is merely by chance (much less than 1 %) that a lightning-active region is within its FOV at the time of the satellite overpass (Zhang et al., 2019). Nevertheless, the long-running dataset (17 full years) offers insight into the long-term storm activity during this period. There seems to be a decreasing trend in the average per flash LNOx over these years based on the -method; although more lightning activity was observed after 2002. TRMM was boosted from 350 km to 402 km in August of 2001.

We compiled nearly 4 years (2017 to September 2020) of quality-controlled ISS-LIS data for estimating LNOx over CONUS using three different values of as explained in the following to illustrate the issue related to the uniqueness of . In the four years under ISS-LIS surveillance, less annual lightning activity was detected by ISS-LIS than in those earlier years by TRMM-LIS over CONUS (top panel in **Figure 10**). This is understandable since ISS is orbiting between $\pm 55^o$ in latitude and TRMM $\pm 38^o$ so TRMM spends more time surveying lower latitudes where lightning is more prevalent. Unfortunately, there was no overlapping period of observation from TRMM-LIS and ISS-LIS to inter-compare the two sets of data directly; they have the same instrument design (ISS-LIS was a back-up for TRMM-LIS), but slightly different orbital altitudes. However, we found disparity in lightning detection between ISS-LIS and TRMM-LIS (more

details in Appendix) following the finding of Zhang et al. (2019) that showed different detection performance in the four quadrants of TRMM-LIS's CCD. Zhang (2020) also presented sensitivity disparity between ISS-LIS and TRMM-LIS. Overall, and for the above differences mentioned, the value would differ between the two domains under the same $\overline{P} = 250$ mol/flash assumption. Given the lack of overlapping observation, we made three LNOx estimates for ISS-LIS using the -method. The first estimate (labeled ISS_TRMM in Fig. 10) is with $= 3.94\text{x}10^{-11}$ from Koshak (2017) for the TRMM-LIS (obtained from observed lightning over CONUS $< 38^0$ N) in 1998. The second estimate (ISS_CONUS) used $= 2.178\text{x}10^{-11}$ which was found by using a reference period of nearly four years of ISS-LIS CONUS observations and assuming a CONUS average $\overline{P} = 250$ mol/flash. The third (ISS_Globe) used $=2.695\text{x}10^{-11}$ obtained from four years of ISS-LIS global observation (i.e. assuming global average $\overline{P} = 250$ mol/flash). Again, all these estimates are based on the upward optical flux F_k discussed above in (2).

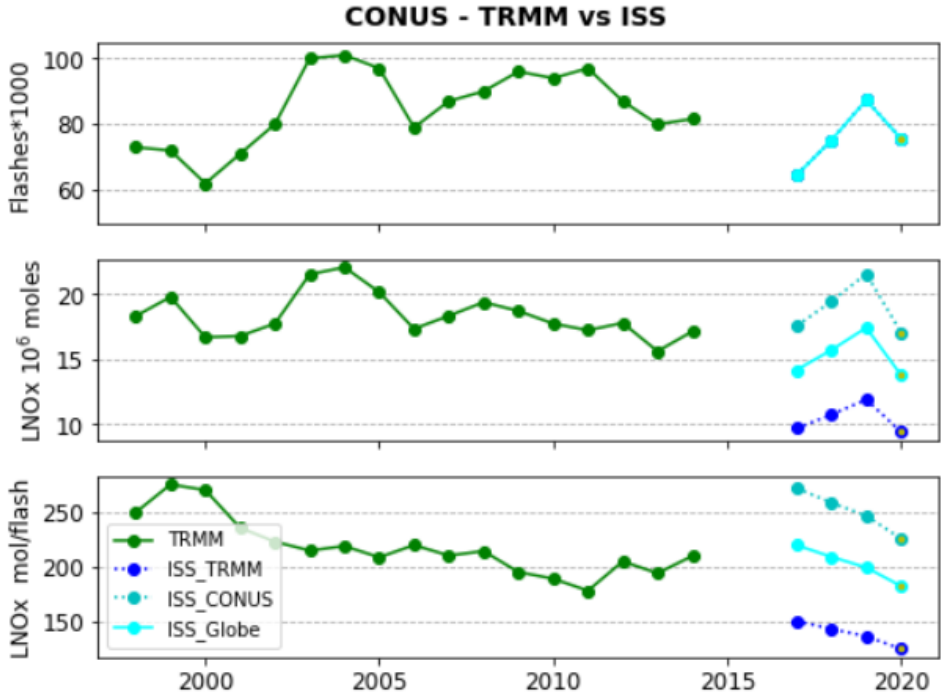

Figure 10. Observed annual lightning flash counts (top panel), and estimated annual LNOx production in annual total (middle) and per flash (bottom) for the CONUS from TRMM-LIS (1998-2014) due to Koshak (2017) and ISS-LIS (2017-2020) from this study. Note that the ISS-LIS data in 2020 only includes the first 9 months. The different estimates for ISS-LIS are in the value. The ISS_Globe and ISS_CONUS use derived from nearly 4 years of ISS-LIS global and CONUS-only observation, respectively.

The annual total LNOx over CONUS is estimated to be ~ (12, 20, 16) mega-moles on average for the (ISS_TRMM, ISS_CONUS, ISS_Globe) estimation. The per-flash values on average are ~ (140, 250, 200) mol/flash for the (ISS_TRMM, ISS_CONUS, ISS_Globe) estimates, respectively. The total LNOx and per flash values obtained from the ISS_Globe estimation fall between the other two estimates (bottom panel in **Figure 10**) and is more acceptable since a larger sample of flashes is used in estimating . Regardless of the magnitude of the per-flash values, all three estimates show a declining trend. This comparison demonstrates the sensitivity of per flash and total values of LNOx on the choice of , and the need for independent observational assessments of .

Moreover, we made a cross-dataset comparison of estimated per flash LNOx over CONUS, comparing estimates obtained from the GLM (as in Sec. 5.1.1) with the ISS-LIS. The comparison results are presented in **Figure 11.** The earlier part of the GLM estimation (prior to Feb. 2019) only used GLM16 data. Note that LIS_Globe uses $= 2.695\text{x}10^{-11}$ as does ISS_Globe, and LIS-CONUS is using $= 2.178\text{x}10^{-11}$ (same as ISS_CONUS). Also, note that a GLM flash is quite comparable to a LIS flash as both instruments are in the same heritage line and the GLM event/group/flash clustering algorithm follows that for LIS. A factor that may cause a significant difference between the two flashes is the footprint size (4km at nadir for ISS-LIS compared to 8km at nadir for GLM) and the threshold to identify a cloud top illumination as a lightning event. The comparisons in **Figure 11** show a largely consistent seasonal/monthly variation of average per flash LNOx across all estimates. Compared to the GLM estimates, the ISS-LIS estimates show more per flash LNOx variation from one month to the next. It should be noted that the value in the GLM estimates was derived from flashes in a domain covering most of N. America and nearby waters.

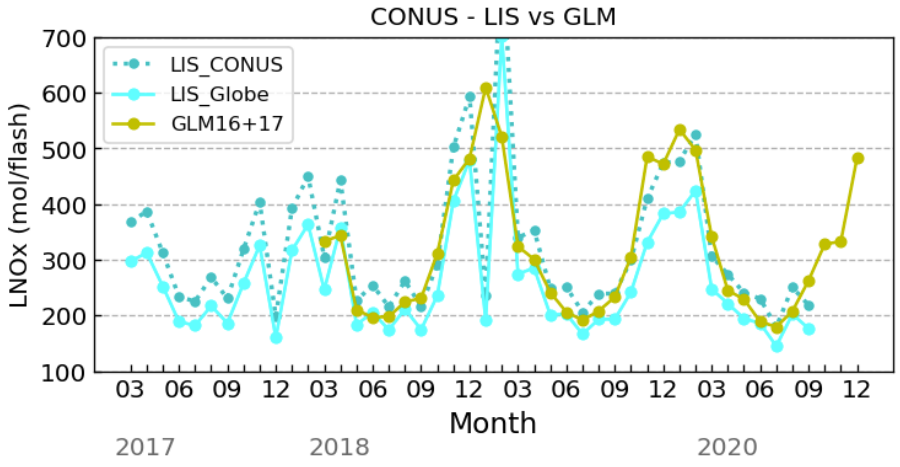

Figure 11. Estimated LNOx per flash production for the CONUS from GLM and ISS-LIS observations based on the -method.

The key conclusion to be drawn from these comparisons is that acts as a scaling factor linked to the assumed average production rate $\overline{P}$. This assumption requires a large number of flashes over diverse geographical regions and over a long period of time for each observation platform. The values used for ISS-GLOBE (= 2.695x10^{-11}) and GLM16+17 (=1.5336x10^{-22}) estimates in **Figures 10** and 11 better satisfy these conditions and are more reliable for respective platforms. The value for GLM16+17 will be further refined in the future as more GLM observations become available.

As stated in the previous sections, the values can be further verified with modeling and/or observation-oriented studies, e.g. exploiting the NO_2 observation from the future TEMPO with simulations of LNOx production generated from the -method. With the formation of both the global satellite constellation of lightning observation (of which GLMs are leading the way) and air pollution monitoring (of which the Korean GEMS is spearheading and TEMPO and the European Sentinel-4 are upcoming), a regional satellite-derived LNOx emissions model can be established and applied for regions in the surveillance of the satellite lightning observation constellation. The ISS-LIS data can be used to help reconcile the parameter regionally and globally.

Z-ratio

Among those matched GLM16/17 flashes, about 13/17% are matched to more than one NLDN-CG flash. If we invert the matched/unmatched ratio we obtain the value of 2.94-3.70, which is comparable to but a bit higher than the IC:CG ratio (referred to as Z-ratio) of 2.64-2.94 from Boccippio et al. (2001) for the CONUS. Considering that 13/17 % of the matched GLM flashes correspond to multiple NLDN-CG flashes, if we take the ratio of the unmatched GLM flashes to the number of NLDN-CG flashes (which would be larger than the GLM matched flashes), the ratio will be lowered to slightly above 3 for combined GLM16 and 17 results and come closer to the Z-ratio estimated by Boccippio et al. (2001).

We are inclined to conclude that we can approximate the Z-ratios by the unmatched/matched ratios as the average numbers are close to those for CONUS from previous studies (Boccippio et al., 2001; Medici et al, 2017; together referred to as BM hereafter) that used much longer-term (4-18.5 yr) datasets. However, the geographical distribution pattern of the unmatched:matched flash ratios we obtained (**Figure 12a**) look quite different compared to those from the BM studies (**Figure 12b**, and also see Figure 8 in Medici et al, 2017).

Many factors may contribute to the disparity between **Figure 12** results and the ratios in BM. The satellite datasets used in BM are from observation onboard LEO satellites and do not have the GLM's edge degradation issues that lead to uneven DE across the continent. TRMM-LIS observations were shown to have higher IC-flash DE (Thomas et al., 2000; Franklin 2013). Furthermore, those LEO satellite sensors with finer resolution and lower detection threshold than

those of the GLM can identify more flashes that would be missed by the GLM (Zhang and Cummins, 2020). The difference may tilt the local ratio significantly.

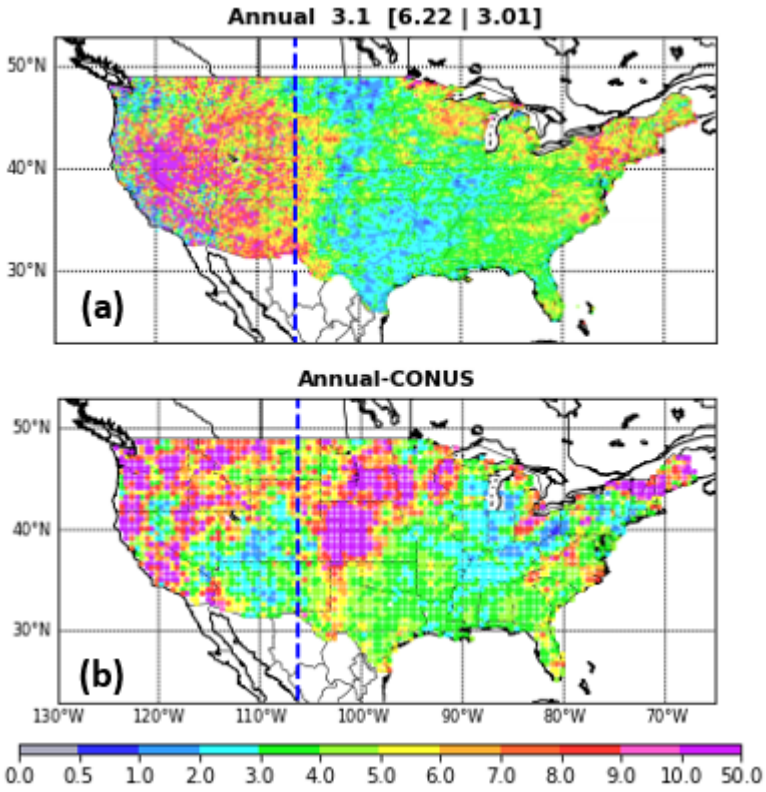

Figure 12. (a) Ratio of unmatched GLM : matched NLDN-CG flashes ratio, (b) IC:CG ratio from Boccippio et al (2001). The three numbers in (a) title bar are the ratio for the overall, west, and east of the 106.2 ^{0}W, respectively.

Furthermore, the NLDN dataset used in this study may have a dissimilar IC/CG classification to those used in BM. In the test of a 21-day NLDN sample (~40x10^6 strokes), the latest upgrade of NLDN classification assigned considerably fewer CG events compared to its 2016 version (53.6/11.5 % decrease in positive/negative CG) and pre-2015 version (19.6/11.6 % decrease in positive/negative CG), while increasing reclassification to IC (Murphy et al., 2021).

For all these reasons, the Z-ratio derived from the GLM/NLDN needs to be further validated. Currently, our LNOx production model offers two options for IC/CG ratio. The first option is the use of a fixed value of 3 for IC:CG ratio for the whole domain. The other option uses the daily (based on calendar date) Z-ratio from Boccippio et al. (2001) for the LNOM model with a future upgrade from Medici et al. (2017).

5.3 Vertical LNOx Profiles

In a gridded domain, the -method can be applied to obtain a two-dimensional (2D) LNOx production distribution for regional storm analyses and broader seasonal analyses. For model simulations, three-dimensional (3D) LNOx production is often required as input for the emission field. To emulate the vertical distribution of this emission field, we adapt the vertical profiles of LNOx production that were generated by the LNOM (Koshak et al., 2009, 2010; Koshak, Peterson, et al., 2014) to distribute LNOx for IC and CG flashes based on the specification of IC and CG flashes in a grid cell (Section 5.2). The profiles were constructed monthly based on laboratory work and multiple years of NLDN and LMA observations. The LNOM-derived vertical LNOx profiling is based not only on the LMA/NLDN observations but also on laboratory results and theoretical parameterizations of LNOx production for various discharge processes (i.e., return-strokes, hot core stepped and dart leaders, stepped leader corona sheaths, K-changes, continuing currents, and M-components).

The resulting IC/CG profiles from the multi-year data fusion in the LNOM show the different vertical core locations of IC/CG, as well as their differential vertical extents in monthly/seasonal fluctuation, deeper in the warm months as the tropopause grows and shallower in the cold months when the tropopause altitude decreases. **Figure 13** shows the example of the IC and CG profiles for July (summer) and December (winter).

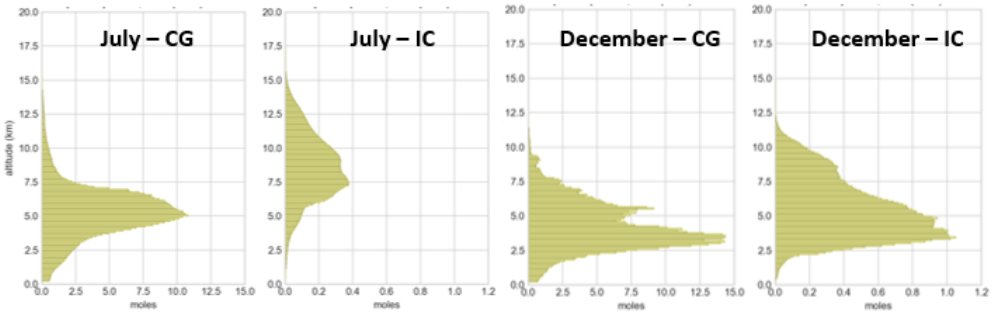

Figure 10. Vertical LNOx profiles for the month of July (top panels) and December (bottom). Vertical increment is 100m.

Figure 13. Vertical LNOx profiles derived from the LNOM (Koshak, 2014) for the month of July and December. Vertical increment is 100m.

Note that the LNOM profiles are adapted to vertically distribute the −method derived LNOx. That is, the total LNOx production in the column over a grid cell is tied to the detected lightning optical energy of the flashes as described by the −method. Then, the NOx is distributed vertically in compliance with the shape of the LNOM profiles.

Summary

In this study, we compiled and evaluated nearly 4 years of GLM16 (March 2018 – December 2021) and 3 years of GLM17 (February 2019 - December 2021) data, and provided the seasonal patterns, geographical variation, land/ocean contrast, and annual fluctuation of the GLM observed lightning activity and flash optical energy. We conducted a matching between NLDN-CG and GLM data to extract insight into the lightning characteristics of CG and IC flashes in the GLM observations. For the LNOx emission model, we provided an overview of the -method (Koshak, Vant-Hull, et al., 2014; Koshak 2017) and demonstrated the application of the method in regional LNOx production estimation with the geostationary GLM and LEO ISS-LIS observations with some preliminary evaluations. Additionally, we employed vertical profiles of the LNOx production and Z-ratio from LNOM in the emissions model to provide a three-dimensional LNOx emission field for use in chemical transport models. Our findings and results are summarized below:

Our analyses of the GLM data show that lightning activity (flash count) occurred far more frequently over land than over the ocean. As a result, lightning occurrences observed across the full disk coverage of GLM showed a seasonal variation greatly influenced by lightning over land where lightning is more active in the warmer months. In contrast, lightning flash optical energy is higher over the ocean than over land. Over CONUS, both flash count and flash optical energy show a clear seasonal pattern: lightning activity peaks in the summer, and reaches the lowest in the winter. Averaged flash optical energy is highest in January-February at about 2.5-3 times the values around July which is the lowest in a year.

Edge degradation effects of the GLM detection are evident over N. America, and quite symmetric along the middle longitude between the GOES-16 and GOES-17. The degradation appears to be severe toward the FOV edges. On average, 44% (36%) more (less) flashes and 40% (41%) lower (higher) flash optical energy were observed by GLM16 than by GLM 17 over the east (west) of the middle longitude, for a relative measure. To compensate for the degradation, we suggest blending GLM16 and 17 observations for applications using the data over the N. America continent by using GLM17 data for areas west of the middle longitude and GLM16 east of it. GLM instrument artifacts (i.e. horizontal striations described in Section 3) are apparent in certain predictable geographical regions and these artifacts can affect flash optical energy statistics, and hence LNOx estimates. Our future plan is to mitigate these artifacts by applying software filtering techniques. In addition to edge degradation and the striation artifact, low GLM DE is shown over the Rockies from the inter-comparison with the NLDN-CG observation.

Composites of the GLM16 and 17 observations show that lightning activity occurs mostly in E. US with an overwhelming (94%) of lightning flashes occurring east of the Rockies. The most active of all are in Florida. A geographical con-

trast is shown with the diurnal variation in that lightning is more active in the SE coastal states during the daytime and in the Central Plains at night. Two-thirds of the overall lightning flashes are observed in the summer months (JJA). This suggests a potentially large impact of LNOx in the summer months in the US.

From inter-comparison of the NLDN-CG flashes and GLM flashes over CONUS, we found the matched GLM flashes (reflecting CG) with characteristics of longer duration (by ~ 30%), more extension (by ~ 50-70%), and higher optical energy (by 100% brighter) compared to the unmatched (representing IC) on average. The overall unmatched:matched flash ratio is around 3 (for 1-year data) which is close to the Z-ratio based on multi-year lightning observations of NLDN and LEO satellites. However, we found considerable disagreement in geographical distribution between the two ratios. This issue requires further investigation before we can be certain about the ratio to apply it in the emission model.

The -method formulated in Koshak, Vant-Hull, et al. (2014) and Koshak (2017) forms the backbone of our LNOx emission model and was applied to estimate LNOx emissions using the space-based lightning mapper data (both ISS-LIS and GLM). Our summer-long CMAQ simulations using LNOx production generated from this emission model yielded results in agreement with previous studies. The -method also shows a consistent performance across different satellite datasets (GLM and ISS-LIS). With the establishment of the future lightning satellite constellation and air pollution observation constellation, the -method for different satellite datasets can be further verified for a regional and global satellite-derived LNOx emissions model.

For the 3-D emission field in a grid cell, we continued to use the Z-ratio from LNOM to attribute IC and CG flashes geographically and seasonally and adapted the LNOx profiles of IC/CG flashes used in LNOM to distribute LNOx production vertically.

Appendix

Regarding the affinity between TRMM-LIS and ISS-LIS, we show some statistical characteristics of the ISS-LIS event data in comparison to those of TRMM-LIS shown in Zhang et al. (2019). With the currently available quality controlled ISS-LIS data (March 2017 – September 2020), the statistics shown here are assembled based on the two full years (2018 and 2019) of the data (**Table A1** and **Figure A1**). The data of the other two non-full years possess very similar statistics while they are not presented here. To comply with the nomenclature used in Zhang et al. (2019), the spectral radiance density (spectral radiance over the 2ms CCD frame) in this appendix will be referred as "radiance density" and shown in [mJ/m^2/sr/nm].

The annual event counts for ISS-LIS are 35.63/34.25 x10^6 for 2018/2019 that are only about half of those observed by TRMM-LIS in 2012 (73.95 x10^6) and

2013 (67.92 x10^6). Given that the ISS is orbiting between 55^0 S and 55^0 N and TRMM was between 38^0 S and 38^0 N, we expect TRMM-LIS oversaw many more lightning activities than would ISS-LIS as there are more lightning occurring in the tropical and subtropical regions than in the mid-latitudes globally. As a matter of fact, 84.4% (83.5%) of the lightning events were found in the tropical-subtropical zone between 38^0 S and 38^0 N and only 15.6% (16.5%) were found beyond this zone for 2018 (2019) in the ISS-LIS data. Tracking the "view-time" parameters in the ISS-LIS dataset, we found roughly only 48% (47.9% for 2018 and 47.5% for 2019) of the observation took place between 38^0 S and 38^0 N. Factoring in the observation time (view time), but without considering the conformity between TRMM-LIS and ISS-LIS orbits over this lower latitude zone, that gives about 15% less event counts for 2018-2019 compared to 2012-2013.

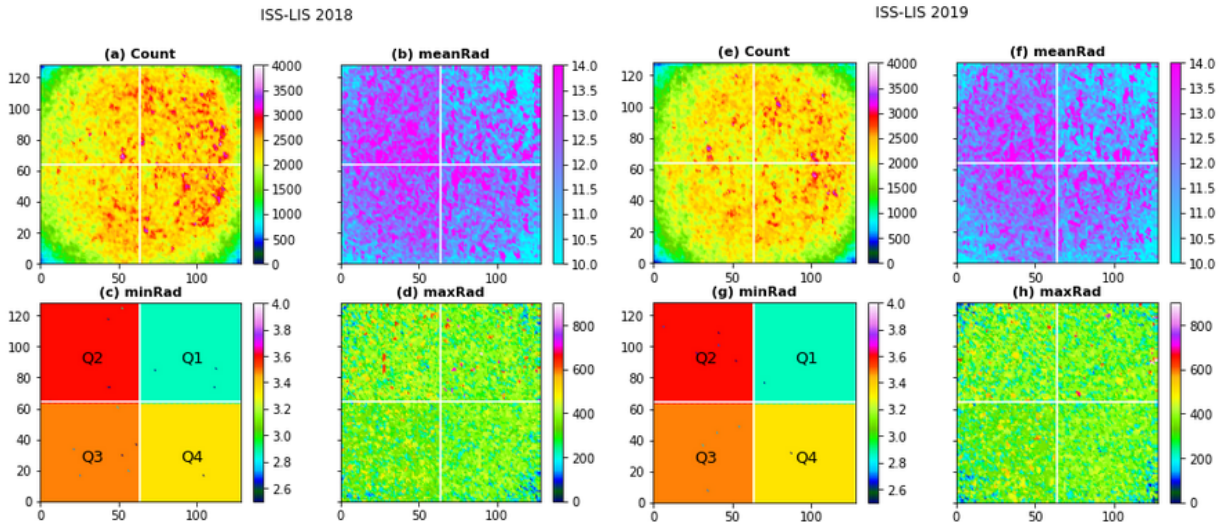

Figure A1. Observed (a) event counts, (b) mean event radiance density, (c) minimum event radiance density, and (d) maximum event radiance density for 2018 in the four quadrants of the ISS-LIS CCD. (e)-(h) same as (a)-(d) but for 2019. The radiance density is in [J/m^2/sr/ m].

Table A1. Statistics of event radiance density in [J/m2/sr/ m] and event count in the four ISS-LIS CCD quadrants for the two full years: 2018 (upper numbers) and 2019(bottom numbers).

	Q1	**Q2**	**Q3**	**Q4**
Mean	12.86	13.44	12.87	12.93
	12.48	13.10	12.52	12.61
Median	6.24	7.20	6.95	6.91
	5.96	7.20	6.95	6.91
Std ( )	23.06	22.21	21.11	22.64
	22.17	20.67	20.31	21.47

	Q1	Q2	Q3	Q4
Skewness	8.39	8.90	9.05	8.70
	8.12	8.81	9.70	8.65
Maximum	366.1	375.0	349.3	352.5
	355.6	356.1	344.5	352.7
Count	9464978	8545074	8489792	9135073
	9021833	8175135	8206120	8832407
Count %	100	90.3	89.7	96.5
	100	90.6	91.0	97.9

The maximum recorded event radiance density (ERD hereafter) over the four ISS-LIS CCD quadrants are (Q1: 885.0, Q2:846.9, Q3: 604.8, Q4: 463.6) mJ/m^2/sr/nm for all 4 years, consistent with those of TRMM-LIS except for Q3 (597.4) for 2018. It suggests those numbers are hard wired upper limits for the quadrants for both LIS instruments and none of the observed ERD reached the upper limit in Q3 for 2018. Similarly, the minimum ERD in the four quadrants are almost uniform (Q1: 2.866, Q2: 3.602, Q3: 3.489, Q4: 3.349), same as those for TRMM-LIS, except a spotty few pixels having minima lower than these numbers as shown in **Figure A1 (c) and (g)**. The minima in some of those spots are zero or near zero suggesting they are nighttime events as the background value for nighttime is zero (Zhang et al., 2019). In comparison, the minimum ERD in the four quadrants for TRMM-LIS were uniform across each quadrant. Similarity with TRMM-LIS mostly stops here.

While the ERD minima and maxima for the four whole quadrants are very different and being quite consistent between TRMM- and ISS-LIS (except the minimum in a few pixels), their actual statistics look significantly different between the two datasets. First of all, the mean lightning event count and mean ERD in Q1 do not stand out as much compared to the other quadrants (**Figure A1**) as for TRMM-LIS shown in figure 1 and 2 in Zhang et al. (2019). Similar to the TRMM-LIS, the right quadrants of ISS-LIS recorded more events than the left quadrants and Q1 had the highest event count. However, quadrants Q2, Q3 and Q4 recorded about 9-10 %, 9-10.5 %, and 2-3.5 % less events, respectively, compared to Q1 (**Table A1**). These numbers are much lower than those (~ 18 %, ~16 %, ~12 %), at about half or less, for TRMM-LIS. Furthermore, although individual pixel mean ERD seems a bit lowered in Q1 (**Figure A1** (b) and (f)) the overall mean ERD for the four quadrants are comparable in the case of ISS-LIS (12.86 to 13.44 mJ/m^2/sr/nm for 2018 and 12.48 to 13.10 mJ/m^2/sr/nm for 2019), with the differences among them being statistically insignificant (0.4 to 3.5 %). In contrast, the mean ERD was significantly lower for Q1 (12.21 to 12.37 mJ/m^2/sr/nm) compared to other quadrants (13.94 to 14.50 mJ/m^2/sr/nm) by 8 to 15 % in 2012 and 2013 in the case of TRMM-LIS data (Zhang et al., 2019).

Expectedly, the ERD distribution is highly skewed in all four quadrants, with

skewness of 8 to 10 as illustrated by the much larger maxima compared to the mean and median values. The mean values being about twice as large as the medians indicates the large and positive skewness, as well.

The maximum ERD for each pixel in the quadrants, shown in **Figure A1** (d) and (h), appear similarly chaotically distributed in all four quadrants and their mean values are in similar magnitude ($\overline{\text{Maximum}}$

in **Table A1**). The exceptions are that Q3 saw few pixels and Q4 saw none with maximum ERD getting close to ~ 600 mJ/m^2/sr/nm as their upper limit are 604.8 and 463.6 mJ/m^2/sr/nm, respectively. Even so, the mean maximum ERD in Q4 is not depressed compared to all the other quadrants as in TRMM-LIS.

For only the events observed between 38^0 S and 38^0 N (**Table A2**), we see very similar statistics to that of the all events (**Table A1**), although with slightly smaller mean values. The event count in Q2, Q3, and Q4 is closer to that in Q1 compared to the all-events scenario, increasing the contrast to the TRMM-LIS.

To summarize, the four quadrants of ISS-LIS CCD have the same upper and lower ERD limits as TRMM-LIS CCD. Its Q1 quadrant also records (detects) more lightning events compared to the other three quadrants as did the Q1 quadrant of TRMM-LIS. However, the differences are much smaller compared to those in TRMM-LIS. Moreover, unlike in TRMM-LIS, the four quadrants show similar mean and maximum ERD in the case of ISS-LIS despite the very different lower and upper limits for each quadrant.

Table A2. Same as **Table A1,** but for data observed between 38^0 S and 38^0 N.

	Q1	**Q2**	**Q3**	**Q4**
Mean	12.57	13.35	12.73	12.79
	12.39	13.10	12.47	12.52
Median	6.07	7.20	6.95	6.91
	5.89	7.20	6.95	6.90
Std ( )	23.13	22.67	21.49	22.68
	22.42	21.32	20.70	21.73
Skewness	8.73	8.82	9.04	8.89
	8.13	8.62	9.73	8.78
$\overline{\text{Maximum}}$	357.5	363.8	339.7	345.0
	343.3	339.5	333.9	342.2
Count	7890926	7265489	7228182	7680339
	7493717	6815003	6880846	7396022
Count %	100	92.1	91.6	97.3
	100	90.9	91.8	98.7

Acknowledgments

This work was made possible by the *Earth from ISS – LIS* program at NASA Headquarters [Program Manager Will McCarty, and Program Executive Jamie Wicks]. We are also grateful to the ISS-LIS Principal Investigator at the NASA Marshall Space Flight Center, Dr. Timothy Lang for his guidance and support (UAH Cooperative Agreement 80MSFC22M001) through all phases of this work effort. In addition, a portion of the work by co-author Koshak was supported by the Precipitation & Lightning Work Package for the Internal Science Funding Model (ISFM) project *Lightning as an Indicator of Climate* under NASA Headquarters (Dr. Jack Kaye, and Dr. Lucia Tsaoussi), that in part supports NASA's participation in the National Climate Assessment (NCA). Koshak's work on this effort pertaining to GLM-16/17 inter-comparisons was supported by the NOAA GOES-R Series Program (Calibration & Algorithm Working Groups) under Drs. Dan Lindsey and Jaime Daniels. The authors gratefully acknowledge Vaisala Inc. for providing the NLDN data used in this study, as part of the Marshall Mentored Project (MMP, ID #02). The findings presented here were accomplished under partial support from NASA Science Mission Directorate Applied Sciences Program (NASA Grant 80NSSC18K1598). Note the results in this study do not necessarily reflect policy or science positions by the funding agencies.

Open Research

- The GLM data used in this study are available publically and can be found on Google Cloud. For GLM16 the data are located under gs://gcp-public-data-goes-16/GLM-L2-LCFA/ and for GLM17 gs://gcp-public-data-goes-17/GLM-L2-LCFA/.
- The ISS-LIS data is Post-QC Version 1.0 (Blakeslee, 2020) and available online publically from the NASA Global Hydrometeorology Resource Center DAAC.
- The NLDN data is Version 3, provided by Vaisala Inc.

References:

Aich, V., Holzworth, R. H., Goodman, S. J., Kuleshov, Y., Price, C., & Williams, E. R. (2018). Lightning: A new essential climate variable. *Eos*, 99. https://doi.org/10.1029/2018EO104583

Allen, D. J. and Pickering, K. E. (2002). Evaluation of lightning flash rate parameterizations for use in a global chemical transport model. *J. Geophys. Res.-Atmos.*, 107, ACH 15-1–ACH 15-21, https://doi.org/10.1029/2002JD002066, 2002.

Allen, D., Pickering, K. E., Duncan, B., & Damon M. (2010). Impact of lightning NO emissions on North American photochemistry as determined using

the Global Modeling Initiative (GMI) model, *J. Geophys. Res., 115*, D22301, doi:10.1029/2010JD014062

Allen, D. J., Pickering, K. E., Pinder, R. W., Henderson, B. H., Appel, K. W., & Prados, A. (2012). Impact of lightning-NO on eastern United States photochemistry during the summer of 2006 as determined using the CMAQ model. *Atmos. Chem. Phys., 12*, 1737–1758, https://doi.org/10.5194/acp-12-1737-2012

Barthe, C. & Barth, M. C. (2008). Evaluation of a new lightning-produced NOx parameterization for cloud resolving models and its associated uncertainties. *Atmos. Chem. Phys.*, *8*(16), 4691–4710. https://doi.org/10.5194/acp-8-4691-2008.

Bateman, M., and D. Mach (2020). Preliminary detection efficiency and false alarm rate assessment of the Geostationary Lightning Mapper on the GOES-16 satellite. *J. Appl. Remote Sens.*, *14*, 032406, https://doi.org/10.1117/1.JRS.14.032406.

Bateman, M., Mach, D., & Stock, M. (2021). Further investigation into detection efficiency and false alarm rate for the geostationary lightning mappers aboard GOES-16 and GOES-17. Earth and Space Science, 8, 2020EA001237. https://doi.org/10.1029/2020EA001237

Beirle, S., Koshak, W., Blakeslee, R., & Wagner, T. (2014). Global patterns of lightning properties derived by OTD and LIS. *Nat. Hazards Earth Syst. Sci., 14*(10), 2715–2726. https://doi.org/10.5194/nhess-14-2715-2014

Biazar, A. P., & McNider, R. T. (1995). Regional estimates of lightning production of nitrogen oxides. *J. Geophys. Res.-Atmos.*, 100(D11), 22861-22874. https://doi.org/10.1029/95JD01735

Blakeslee, R. J. (2020). Quality Controlled Lightning Imaging Sensor (LIS) on International Space Station (ISS) Science Data [2017-2020]. Dataset available online from the NASA Global Hydrometeorology Resource Center DAAC, Huntsville, Alabama, U.S.A. DOI: http://dx.doi.org/10.5067/LIS/ISSLIS/DATA108

Blakeslee, R. J., Lang, T. J., Koshak, W. J., Buechler, D., Gatlin, P., Mach, D. M., et al. (2020). Three years of the Lightning Imaging Sensor onboard the International Space Station: Expanded global coverage and enhanced applications. *J. Geophys. Res.-Atmos., 125*, e2020JD032918. https://doi.org/10.1029/2020JD032918

Boccippio, D. J., Cummins, K. L., Christian, H. J., & Goodman, S. J. (2001). Combined satellite- and surface-based estimation of the intracloud–cloud-to-ground lightning ratio over the continental United States. *Mon. Wea. Rev., 129*, 108–122, doi:10.1175/1520-0493 (2001)129,0108:CSASBE.2.0.CO;2

Bruning, E. C., & MacGorman, D. R. (2013). Theory and observations of controls on lightning flash size spectra. *J. Atmos. Sci., 70*(12), 4012-4029. Re-

trieved Apr 14, 2022, from https://journals.ametsoc.org/view/journals/atsc/70/12/jas-d-12-0289.1.xml

Chronis, T., Koshak, W., and E. McCaul, E. (2016), Why do oceanic negative cloud-to-ground lightning exhibit larger peak current values?. *J. Geophys. Res. Atmos., 121*, 4049–4068, doi:10.1002/2015JD024129

Cooray, V., Rahman, M., & Rakov, V. (2009). On the NOx production by laboratory electrical discharges and lightning. *J. Sol. Atmos. Terr. Phys. 71*, 1877–1889.

DeCaria, A. J., Pickering, K. E., Stenchikov, G. L., & Ott, L. E. (2005). Lightning-generated NOx and its impact on tropospheric ozone production: A three-dimensional modeling study of a Stratosphere-Troposphere Experiment: Radiation, Aerosols and Ozone (STERAO-A) thunderstorm. *J. Geophys. Res.-Atmos., 110*(D14). https://doi.org/10.1029/2004JD005556

Deierling, W., Petersen, W. A., Latham, J., Ellis, S., & Christian, H. J. (2008). The relationship between lightning activity and ice fluxes in thunderstorms. *J. Geophys. Res.-Atmos., 113*, D15210, doi:10.1029/2007JD009700

Goodman, S. J., Blakeslee, R. J., Koshak, W. J., Mach, D., Bailey, J., Buechler, D., Carey, L., Schultz, C., Bateman, M., McCaul Jr, E., & Stano, G., (2013). The GOES-R geostationary lightning mapper (GLM). *Atmos. Res., 125*, pp.34-49. https://doi.org/10.1016/j.atmosres.2013.01.006

Finney, D. L., Doherty, R. M., Wild, O., Huntrieser, H., Pumphrey, H. C., & Blyth, A. M. (2014). Using cloud ice flux to parametrize large-scale lightning, *Atmos. Chem. Phys., 14*, 12665–12682, https://doi.org/10.5194/acp-14-12665-2014

Finney, D. L., Doherty, R. M., Wild, O., Young, P. J., & Butler, A. (2016). Response of lightning NOx emissions and ozone production to climate change: Insights from the Atmospheric Chemistry and Climate Model Intercomparison Project. *Geophys. Res. Lett., 43*(10), 5492–5500. https://doi.org/10.1002/2016GL068825

Franklin, V. (2013). An Evaluation of the Lightning Imaging Sensor with New Insights on the Discrimination of Lightning Flash and Stroke Detectability, (Master Thesis). University of Alabama-Huntsville.

Franzblau, E., & Popp, C. J. (1989). Nitrogen oxides produced from lightning. *J. Geophys. Res.-Atmos., 94*(D8), 11089-11104.

Gallardo, L. & Cooray, V. (1996). Could cloud-to-cloud discharges be as effective as cloud-to-ground discharges in producing NOx?. *Tellus B: Chem. Phys.l Meteor.,* 48:5, 641-651, DOI: 10.3402/tellusb.v48i5.15937

Hansen, A. E. (2012). Development of a regional lightning nitrogen oxide parameterization for the weather and research forecast chemistry model (Doctoral Dissertation). The Florida State University.

Kang, D., Pickering, K. E., Allen, D. J., Foley, K. M., Wong, D. C., Mathur, R., & Roselle, S. J. (2019a). Simulating lightning NO production in CMAQv5.2: evolution of scientific updates. *Geosci. Model Dev., 12*, 3071–3083, https://doi.org/10.5194/gmd-12-3071-2019

Kang, D., Foley, K. M., Mathur, R., Roselle, S. J., Pickering, K. E., & Allen, D. J. (2019b). Simulating lightning NO production in CMAQv5. 2: performance evaluations. *Geosci. Model Dev.*, 12(10), 4409-4424, https://doi.org/10.5194/gmd-12-4409-2019

Kang, D., Mathur, R., Pouliot, G.A., Gilliam, R.C. and Wong, D.C. (2020). Significant ground-level ozone attributed to lightning-induced nitrogen oxides during summertime over the Mountain West States. NPJ climate and atmospheric science, 3(1), pp.1-7.

Koshak, W. J. (2014). Global Lightning Nitrogen Oxides Production, Chapter 19 of The Lightning Flash, 2nd Edition, editor Vernon Cooray, ISBN: 978-1-84919-691-8, pp. 928, 2014.

Koshak, W. J. (2017). *Lightning NOx estimates from space-based lightning imagers*. 16th Annual Community Modeling and Analysis System (CMAS) Conference. https://ntrs.nasa.gov/api/citations/20170010354/downloads/20170010354.pdf

Koshak, W. J., & H. Peterson (2011). *A summary of the NASA Lightning Nitrogen Oxides Model (LNOM) and recent results.* 10th Annual Community Modeling and Analysis System (CMAS) Conference, http://www.cmascenter.org/conference/2011/agenda.cfm. https://ntrs.nasa.gov/api/citations/20120001523/d

Koshak, W. J., M. N. Khan, A. P. Biazar, M. Newchurch, & R. T. McNider (2009). *A NASA model for improving the lightning NOx emission inventory for CMAQ*. Joint Session: 4th Conference on the Meteorological Applications of Lightning Data and the 11th Conference on Atmospheric Chemistry; 89th Annual AMS Conference. https://ams.confex.com/ams/pdfpapers/147334.pdf

Koshak, W. J., Mach, D., Bateman, M., Armstrong, P., and Virts., K. (2018). GOES-16 GLM Level 2 Data Full Validation Data Quality. *Product Performance Guide For Data Users*. https://www.noaasis.noaa.gov/GOES/PS_PVR2.html#parentHorizontalTab4

Koshak, W. J., H. S. Peterson, E. W. McCaul, A. Biazar (2010). *Estimates of the lightning NOx profile in the vicinity of the North Alabama Lightning Mapping Array*, 21st International Lightning Detection Conference. https://www.google.com/url?sa=t&rct=j&q=&esrc=s&source=web&cd=&ved=2ahUKEwidsaZwqv4AhVomWoFHSKzAwMQFnoECAYQAQ&url=https%3A%2F%2Fwww.vaisala.com%2Fsites%2Fdefaul ZI9a_XTL0j

Koshak, W. J., H. Peterson, M. Khan, A. Biazar, L. Wang (2011). *The NASA Lightning Nitrogen Oxides Model (LNOM): Application to Air Quality Modeling.* XIV International Conference on Atmospheric Electricity.

Koshak, W., Peterson, H., Biazar, A., Khan, M, and Wang, L. (2014a). The NASA Lightning Nitrogen Oxides Model (LNOM): Application to air quality

modeling. *Atmos. Res., 135-136*, 363–369. https://doi.org/10.1016/j.atmosres.2012.12.015

Koshak, W. J., Vant-Hull, B., McCaul, E. W., and Peterson, H. S. (2014b). *Variation of a Lightning NOx Indicator for National Climate Assessment*. XV International Conference on Atmospheric Electricity.

Lapierre, J. L., Laughner, J. L., Geddes, J. A., Koshak, W. J., Cohen, R. C., & Pusede, S. E. (2020). Observing U.S. regional variability in lightning NO2 production rates. *J. Geophys. Res.-Atmos., 125*, e2019JD031362. https://doi.org/10.1029/2019JD031362

Mach, D. M., (2020). Geostationary Lightning Mapper clustering algorithm stability. *J. Geophys. Res. Atmos., 125*, e2019JD031900. https://doi.org/10.1029/2019JD031900

Marchand, M., Hilburn, K., and Miller, S. D. (2019). Geostationary lightning mapper and Earth networks lightning detection over the contiguous United States and dependence on flash characteristics. *J. Geophys. Res.-Atmos., 124*, 11,552-11,567. https://doi.org/10.1029/2019JD031039

Marais, E. A. and Jacob, D. J. and Choi, S. and Joiner, J. and Belmonte-Rivas, M. and Cohen, R. C. and Beirle, S. and Murray, L. T. and Schiferl, L. D. and Shah, V. and Jaegle, L. (2018). Nitrogen oxides in the global upper troposphere: interpreting cloud-sliced NO_2 observations from the OMI satellite instrument. *Atmos. Chem. Phys., 18*(23), 17017 – 17027. https://acp.copernicus.org/articles/18/17017/2018/

Medici, G., Cummins, K. L., Cecil, D. J., Koshak, W. J., & Rudlosky, S. D. (2017). The intracloud lightning fraction in the contiguous United States. *Mon. Wea. Rev., 145*(11), 4481–4499. https://doi.org/10.1175/MWR-D-16-0426.1

Miyazaki, K., Eskes, H. J., Sudo, K., & Zhang, C. (2014). Global lightning NO x production estimated by an assimilation of multiple satellite data sets. *Atmos. Chem. Phys., 14*(7), 3277-3305. https://doi.org/10.5194/acp-14-3277-2014

Murphy, M. J., and Said, R. K. (2020). Comparisons of lightning rates and properties from the U.S. National Lightning Detection Network (NLDN) and GLD360 with GOES-16 Geostationary Lightning Mapper and Advanced Baseline Imager data. *J. Geophys. Res.-Atmos., 125*, e2019JD031172. https://doi.org/10.1029/2019JD031172

Murphy, M. J., Cramer, J. A., Said, R. K. (2021). Recent history of upgrades to the US National Lightning Detection Network. *J. Atmo. Oceanic. Tech., 38*, 573-585. https://doi.org/10.1175/JTECH-D-19-0215.1

Myhre, G., Shindell, D., and Pongratz D. (2014) Anthropogenic and natural radiative forcing. In Climate change 2013: the physical science basis; *Working Group I contribution to the fifth assessment report of the Intergovernmental Panel on Climate Change* (pp. 659-740). Cambridge, UK and New York, NY: Cambridge Univ. Press.

Nag, A., Murphy, M. J., Cummins, K. L., Pifer, A. E., & Cramer, J. A. (2014, March). Recent evolution of the US National lightning detection network. 23rd Int. Lightning Detection Conf., Tucson, AZ, Vaisala, 6 pp.

Nault, B. A., Laughner, J. L., Wooldridge, P. J., Crounse, J. D., Dibb, J., Diskin, G., et al. (2017). Lightning NOx emissions: Reconciling measured and modeled estimates with updated NOx chemistry. *Geophys. Res. Lett., 44*(18), 9479–9488. https://doi.org/10.1002/2017GL074436

Ott, L. E., Pickering, K. E., Stenchikov, G. L., Allen, D. J., DeCaria, A. J., Ridley, B., et al. (2010). Production of lightning NOx and its vertical distribution calculated from three-dimensional cloud-scale chemical transport model simulations. *J. Geophys. Res.-Atmos., 115*(D4), D04301. https://doi.org/10.1029/2009JD011880

Peterson, H. S. and Beasley, W. H. (2011). Possible catalytic effects of ice particles on the production of NOx by lightning discharges, *Atmos. Chem. Phys., 11*, 10259–10268, https://doi.org/10.5194/acp-11-10259-2011

Peterson, H., & Hallett, J. (2012). Ice particle growth in the presence of nitric oxide. *J. Geophys. Res.-Atmos.,117*(D6). https://doi.org/10.1029/2011JD016986

Peterson, M., Rudlosky, S., & Deierling, W. (2017). The evolution and structure of extreme optical lightning flashes. *J. Geophys. Res.-Atmos., 122*, 13,370–13,386. https://doi.org/10.1002/2017JD026855

Price, C., Penner, J., and Prather, M. (1997). NOx from lightning: 1. Global distribution based on lightning physics, *J. Geophys. Res.-Atmos., 102*, 5929–5941, https://doi.org/10.1029/96JD03504.

Pickering, K. E., E. Bucsela, D. Allen, A. Ring, R. Holzworth, and N. Krotkov (2016), Estimates of lightning NOx production based on OMI NO2 observations over the Gulf of Mexico, *J. Geophys. Res.-Atmos., 121*, 8668–8691, doi:10.1002/2015JD024179.

Rakov, V. A. and Uman, M. A. (2003). *Lightning: Physics and Effects*. New York, NY: Cambridge Univ. Press.

Romps, D. M., Seeley, J. T., Vollaro, D., and Molinari, J. (2014). Projected increase in lightning strikes in the United States due to global warming, *Science, 346*, 851–854. https://doi.org/10.1126/science.1259100, 2014.

Rudlosky, S. D. & Shea, D. T. (2013). Evaluating WWLLN performance relative to TRMM/LIS. *Geophys. Res. Lett., 40*, 2344–2348. https://doi.org/10.1002/grl.50428

Rudlosky, S. D., Goodman, S. J., Virts, K. S., & Bruning, E. C. (2019). Initial geostationary lightning mapper observations. *Geophys. Res. Lett., 46*, 1097–1104. https://doi.org/10.1029/2018GL081052

Rudlosky, S. D., & Virts, K. S. (2021). Dual Geostationary Lightning Mapper Observations, *Mon. Wea. Rev., 149*(4), 979-998. Retrieved Feb 15, 2022,

from https://journals.ametsoc.org/view/journals/mwre/149/4/MWR-D-20-0242.1.xml

Rutledge, S. A., Hilburn, K. A., Clayton, A., Fuchs, B., & Miller, S. D. (2020). Evaluating Geostationary Lightning Mapper flash rates within intense convective storms. *J. Geophys. Res.-Atmos.,125*, e2020JD032827. https://doi.org/10.1029/2020JD032827

Sicard, P. (2021). Ground-level ozone over time: an observation-based global overview. *Curr. Opin. Environ. Sci. Health, 19*, 100226.

Thomas, R. J., Krehbiel, P. R., Rison, W., Hamlin, T., Boccippio, D. J., Goodman, S. J., & Christian, H. J. (2000). Comparison of ground-based 3-dimensional lightning mapping observations with satellite-based LIS observations in Oklahoma. *Geophys. Res. Lett., 27*(12), 1703–1706. https://doi.org/10.1029/1999GL010845

Virts, K. S., & Koshak, W. J. (2020). Mitigation of Geostationary Lightning Mapper Geolocation Errors. *J. Atmo. Oceanic. Tech., 37*(9), 1725-1736. Retrieved Feb 15, 2022, from https://journals.ametsoc.org/view/journals/atot/37/9/jtechD190100.xml

Zhang, D. (2020). *An Evaluation Study of the International Space Station Lightning Imaging Sensor*. AGU 2020 Fall Meeting. https://agu.confex.com/agu/fm20/meetingapp.cgi/Paper/66852

Zhang, D., & Cummins, K. L. (2020). Time evolution of satellite-based optical properties in lightning flashes, and its impact on GLM flash detection. *J. Geophys. Res.-Atmos., 125*, e2019JD032024. https://doi.org/10.1029/2019JD032024

Zhang, X., Yin, Y., van der A, R., Lapierre, J. L., Chen, Q., Kuang, X., Yan, S., Chen, J., He, C., and Shi, R. (2020). Estimates of lightning NOx production based on high-resolution OMI NO2 retrievals over the continental US, *Atmos. Meas. Tech., 13*, 1709–1734, https://doi.org/10.5194/amt-13-1709-2020

Zhao, C., Wang, Y., Choi, Y., & Zeng, T. (2009). Summertime impact of convective transport and lightning NO x production over North America: modeling dependence on meteorological simulations. *Atmos. Chem. Phys., 9*(13), 4315-4327. https://doi.org/10.5194/acp-9-4315-2009

Zhu, Q., Laughner, J. L., & Cohen, R. C. (2019). Lightning NO2 simulation over the contiguous U.S. and its effects on satellite NO2 retrievals. *Atmos. Chem. Phys.. 19,* 13067–13078, 2019. https://doi.org/10.5194/acp-19-13067-2019